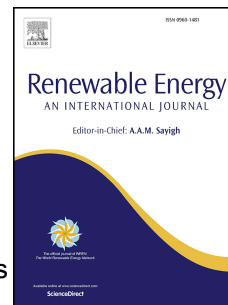


# Accepted Manuscript

Olefin oligomerisation over nanocrystalline MFI-based micro/mesoporous zeotypes synthesised via bottom-up approaches

Andreia F. Silva, Auguste Fernandes, Margarida M. Antunes, Maria F. Ribeiro, Carlos M. Silva, Anabela A. Valente



PII: S0960-1481(19)30163-6

DOI: <https://doi.org/10.1016/j.renene.2019.02.019>

Reference: RENE 11151

To appear in: *Renewable Energy*

Received Date: 12 July 2018

Revised Date: 5 November 2018

Accepted Date: 5 February 2019

Please cite this article as: Silva AF, Fernandes A, Antunes MM, Ribeiro MF, Silva CM, Valente AA, Olefin oligomerisation over nanocrystalline MFI-based micro/mesoporous zeotypes synthesised via bottom-up approaches, *Renewable Energy* (2019), doi: <https://doi.org/10.1016/j.renene.2019.02.019>.

This is a PDF file of an unedited manuscript that has been accepted for publication. As a service to our customers we are providing this early version of the manuscript. The manuscript will undergo copyediting, typesetting, and review of the resulting proof before it is published in its final form. Please note that during the production process errors may be discovered which could affect the content, and all legal disclaimers that apply to the journal pertain.

# Oligomerisation of 1-Butene Continuous-flow operation

## MFI Zeotypes - Bottom-up synthetic approaches

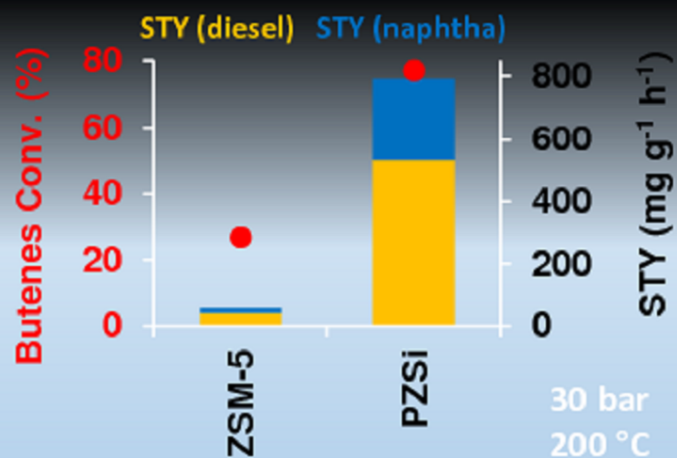
PZSi catalyst

Nanocrystallites

Mesoporosity

Enhanced ratio

L/B acid sites



1 *Revised Manuscript for* RENEWABLE ENERGY.....03/11/2018

2

3 **Olefin oligomerisation over nanocrystalline MFI-based micro/mesoporous**  
4 **zeotypes synthesised via bottom-up approaches**

5

6 Andreia F. Silva,<sup>[a]</sup> Auguste Fernandes,<sup>[b]</sup> Margarida M. Antunes,<sup>[a]</sup> Maria F. Ribeiro,<sup>[b]</sup> Carlos M.  
7 Silva,<sup>[a]</sup> and Anabela A. Valente\*<sup>[a]</sup>

8

9 <sup>a</sup> CICECO - Aveiro Institute of Materials, Department of Chemistry, University of Aveiro, Campus  
10 Universitário de Santiago, 3810-193 Aveiro, Portugal. E-mail: atav@ua.pt

11 <sup>b</sup> Institute for Biotechnology and Bioengineering, Centre for Biological and Chemical Engineering,  
12 Instituto Superior Técnico, Av. Rovisco Pais, 1049-001 Lisboa, Portugal

13

14

15 **Abstract**

16 The oligomerisation of 1-butene was studied under high-pressure continuous-flow conditions (200-  
17 250 °C, 30-40 bar), in the presence of micro/mesoporous zeotypes based on the MFI topology, which  
18 were prepared via different non-destructive bottom-up strategies: crystallisation of silanized  
19 protozeolitic units; co-templating with a dual function (polymeric) template; and using a sole  
20 structure directing agent (non-surfactant and non-polymeric) to generate mesoporosity. The synthesis  
21 method influenced the material properties and consequently the catalytic performance. In targeting  
22 hydrocarbons with boiling point ranges characteristics of diesel, the zeotypes benefited from regular  
23 morphology, reduced crystallite size, mesoporosity and enhanced molar ratio of Lewis (L) to  
24 Brønsted (B) acid sites (L/B). In general, the zeotypes outperformed commercial zeolite ZSM-5. The  
25 best-performing zeotype was prepared according to the Serrano strategy based on the crystallization

1 of silanized zeolitic seeds, and led to 97 % conversion and an average space-time yield of liquid  
2 products of  $1077 \text{ mg g}_{\text{cat}}^{-1} \text{ h}^{-1}$ , at 250 °C, 40 bar. The zeotypes seemed more stable than the  
3 commercial zeolite, based on molecular level characterization studies of the used/regenerated  
4 catalysts, with some differences in catalytic activity.

5  
6 **Keywords:** 1-butene; oligomerisation; continuous-flow; MFI topology; hierarchical zeotypes;  
7 hydrothermal synthesis

## 9 1. Introduction

10  
11 The importance of developing and implementing efficient and clean processes for fuel production is  
12 evident in an energy-expanding world. Worldwide, transportation is largely based on petroleum and  
13 other liquid fuels obtained from natural gas, coal, or biofuels [1,2]. Projections for 2040 based on the  
14 International Energy Outlook 2016 [1] indicate that gasoline (33 %) and diesel/biodiesel (33 %) remain the largest transportation fuels, followed by jet fuel (14 %), with the remaining 9 % regarding  
15 electricity, residual fuel oil and other liquids. The great dependence of society on fossil fuels is  
16 believed to contribute to global warming, and in mitigating this problem, the solutions may involve  
17 the use of renewable sources of energy, and repurposing industrial byproducts for the production of  
18 chemicals and fuels.

19  
20 Light olefins are byproducts of petrochemical or Fischer-Tropsch processes [3-6], and, on the other  
21 hand, may be obtained from renewable sources, e.g. butenes from carbohydrate biomass [7-9]. The  
22 oligomerisation of light olefins (C2-C5) may be a flexible technology and attractive route to produce  
23 diverse products including synthetic transportation fuels (gasoline, diesel, jet fuel) with reduced  
24 content of sulphur and aromatic compounds, drugs, detergents, lubricants and dyes [10,11]. Olefin  
25 oligomerisation is favoured in the presence of acid catalysts, which should be adequate for

1 continuous-flow processes. In this sense, porous solids possessing significant specific surface area  
2 available for the catalytic reaction, are attractive. On the other hand, olefin oligomerisation involves  
3 the formation of relatively bulky products, and, thus, to facilitate mass transport and maximize the  
4 portion of effectively utilized catalyst in the process, it is desirable that the solid acids possess  
5 sufficiently large pores [12-16].

6 Important industrial solid acid catalysts are porous aluminosilicates. This category of materials is  
7 very versatile: amorphous or crystalline materials with different topologies, morphological, textural  
8 and acid properties may be prepared [17-19]. Most successful types of aluminosilicates applied in the  
9 industry include zeolites, which are crystalline and microporous materials. Zeolites may possess  
10 superior acid properties (e.g. stronger acidity) to amorphous aluminosilicates such as, ordered  
11 mesoporous materials of the type MCM-41, SBA-15 or TUD-1; the latter possess less rigid  
12 frameworks and silanol surface groups, albeit larger pores than zeolites, advantageously allowing  
13 enhanced acid sites accessibility [4,20-24]. Favourable compromise between textural and acid  
14 properties of porous solid acids is important for maximizing product yields. Another important factor  
15 for maximizing catalyst productivity is the catalyst stability. Zeolites possessing the MFI topology  
16 (medium pore, with the channel sizes of  $0.55 \times 0.51 \text{ nm}^2$  and  $0.56 \times 0.53 \text{ nm}^2$ ) are relatively robust  
17 industrial catalysts [25,26] and used in commercial olefin oligomerisation processes [27-31].  
18 However, they may present important mass transfer limitations and suffer fast catalyst deactivation  
19 in the oligomerisation of olefins such as butene [32]. Hence, great attention has been drawn to the  
20 development of aluminosilicate zeotypes with reduced crystallite sizes and/or enlarged pores. The  
21 synthetic strategies for obtaining zeotypes possessing mesoporosity may be classified as top-down or  
22 bottom-up approaches [33-36]. Zeotypes prepared via top-down approaches were studied for olefin  
23 oligomerisation, and possessed superior performances in comparison to conventional microporous  
24 zeolites; the zeotypes were based on the MFI [37-39], MOR [40,41], FAU [42] and TON [43]  
25 topologies.

1 A main difference between the top-down and bottom-up approaches is that the former may be  
2 somewhat destructive compared to the latter. Regarding the bottom-up approaches, several specific  
3 strategies (e.g. with or without addition of structure-directing agents) were reported for preparing  
4 zeotypes based on different topologies and possessing mesoporosity (2-50 nm). Wang et al. [44] and  
5 Yang et al. [45] reported the synthesis of hydrothermally stable zeotypes based on the MFI topology,  
6 via a (soft) co-templating protocol (denoted CoT), which involved the simultaneous use of small and  
7 large cationic ammonium-based hydrophilic templates. The mesoporosity could be fine-tuned by  
8 changing the amount of the large cationic template [44,45]. Serrano et al. [46-48] reported a strategy  
9 (denoted PZSi) based on the crystallization of silanized zeolitic seeds (or protozeolitic units)  
10 possessing MFI topology, which may be followed by a treatment with a basic surfactant-containing  
11 solution (PZSiS) to rearrange the zeolitic units over the mesopore surface. Wan et al. [49] reported a  
12 method not requiring additional template or zeolite seeding crystals (denoted noT). The hierarchical  
13 zeotypes presented superior performances to conventional microporous ZSM-5 for different acid-  
14 catalysed liquid or gas phase reactions, under batch or continuous-flow operation. In particular, the  
15 synthetic approach by Wan et al. [49] led to porous solid acids that enhanced the conversion of  
16 methanol to gasoline, and was more stable towards coking.

17 In this work, the oligomerisation of 1-butene was studied under continuous-flow, and relatively high-  
18 pressure conditions (characteristic of industrial olefin oligomerisation processes [27-31], favouring  
19 the formation of oligomers which involves reduction of the total number of moles of the system), in  
20 the presence of zeotypes based on the MFI topology and possessing mesoporosity. The zeotypes  
21 were prepared via different bottom-up approaches, based on the strategies CoT, PZSi, PSZiS and  
22 noT referred above. The zeotype catalysts were benchmarked (at 200 °C, 30 bar) with commercial  
23 zeolite ZSM-5 possessing Si/Al ratio intermediate of the zeotypes (Si/Al in the range 20-51). Special  
24 attention was given to aspects of catalyst stability.

25

## 1 2. Experimental

### 3 2.1. Materials

4 All reagents and solvents were obtained from commercial sources and used as received. For  
5 materials syntheses: aluminium (III) isopropoxide (AlP; 98 %, Aldrich), sodium aluminate (50-56 %  
6 Al<sub>2</sub>O<sub>3</sub>, Riedel de Haen), tetraethylorthosilicate (TEOS; 98 %, Sigma), tetrapropylammonium  
7 hydroxide solution (TPAOH; 40 wt% in water, Alfa-Aesar), sodium hydroxide (97 %, Sigma-  
8 Aldrich), Poly(acrylamide-co-diallyldimethylammonium chloride) (PDD-AM; 10 % in water,  
9 Aldrich), [3-(Phenylamino)propyl]trimethoxysilane (PHAPTMS; Aldrich),  
10 hexadecyltrimethylammonium bromide (CTAB; 98%, Aldrich), ammonium hydroxide (28-30 %,   
11 Sigma-Aldrich), and ammonium nitrate (98 %, Aldrich).

12 For the catalytic tests: 1-butene (99.6 %, Praxair), nitrogen (Air Liquide), silicon carbide (SiC, Ø  
13 0.31 mm, SIKA), dichloromethane (analytical reagent grade, Fisher Chemical), and n-pentane (95 %,   
14 Fluka).

15 The commercial zeolite NH<sub>4</sub>ZSM-5 (as reference, the molar ratio Si/Al is 25, and the specific surface  
16 area equals 425 m<sup>2</sup> g<sup>-1</sup>, Alfa-Aesar) was tested as benchmark catalyst after calcination at 550 °C  
17 (heating rate of 1 °C min<sup>-1</sup>) in static air during 5 h. The calcined material is denoted ZSM-5(29)  
18 where 29 is the molar ratio Si/Al determined by EDS (discussed ahead).

### 20 2.2. Syntheses of the catalysts

21 The zeotype materials based on the MFI topology were synthesised via bottom-up approaches, and  
22 the prepared materials were denoted as hZSM-5(x)-y, where x is the Si/Al ratio giving by EDS, and  
23 y is the abbreviation of the synthesis method. The synthesis protocols were adapted from the  
24 literature [44,46,49]. The protocols/conditions of the synthesized zeotypes are summarised in Table  
25 1.

1

2 2.2.1. *Catalyst hZSM-5(31)-noT*

3 The free template method was carried out following a similar procedure to that described by Wan et  
4 al. [49] Specifically, 0.33 mmol of NaAlO<sub>2</sub>, 12.7 mmol of TPAOH solution (40 % in H<sub>2</sub>O) and 2148  
5 mmol of milliQ-water were mixed and stirred at room temperature for 30 min. Then, 32.9 mmol of  
6 TEOS was added dropwise. The molar composition of the synthesis-gel was 1Al<sub>2</sub>O<sub>3</sub>: 101SiO<sub>2</sub>:  
7 1.34Na<sub>2</sub>O: 39TPAOH: 7215 H<sub>2</sub>O. The resulting mixture was stirred at room temperature for 22 h in  
8 order to obtain a uniform gel, followed by crystallisation at 180 °C for 48 h in a PTFE-lined  
9 stainless-steel autoclave, under static, hydrothermal conditions. After cooling, the resultant product  
10 was recovered by centrifugation, washed thoroughly with milliQ-water and dried at 100 °C  
11 overnight. The solid was gently grinded using an Agate mortar and pestle, and calcined at 550 °C in  
12 static air for 5 h (heating rate of 1 °C min<sup>-1</sup>). The protonic form was obtained by ion-exchange with  
13 1.0 M NH<sub>4</sub>NO<sub>3</sub> aqueous solution (1 g of calcined sample per 10 mL of solution), at 50 °C, under  
14 stirring. The solution was renewed two times, every 24 h. Finally, the solid was centrifuged, washed  
15 with milliQ water, dried at 100 °C over-night, and calcined at 500 °C in static air for 5 h (heating rate  
16 of 1 °C min<sup>-1</sup>), giving a material denoted hZSM-5(31)-noT (noT stands for no additional template).

17

18 2.2.2. *Catalysts hZSM-5(x)-PZSi and hZSM-5(47)-PZSiS*

19 The method of silanization of protozeolitic units was employed following a similar procedure to that  
20 described by Serrano et al. [46] Specifically, the precursor ZSM-5 solution was prepared by mixing  
21 8.11 mmol of TPAOH, 928 mmol of milliQ-water, 42.3 mmol of TEOS and 0.71 mmol of AiP for  
22 hZSM-5(51)-PZSi or 1.41 mmol of AiP for hZSM-5(20)-PZSi; the molar composition of the  
23 synthesis-gel was 1Al<sub>2</sub>O<sub>3</sub>: 120SiO<sub>2</sub>: 23TPAOH: 3000 H<sub>2</sub>O for hZSM-5(51)-PZSi and 1Al<sub>2</sub>O<sub>3</sub>:  
24 60SiO<sub>2</sub>: 11.5TPAOH: 1500 H<sub>2</sub>O for hZSM-5(20)-PZSi. For the two materials, the mixture was aged  
25 at room temperature for 44 h and precrystallized under reflux and stirring (100 rpm) at 90 °C for 22



1 h. The resulting protozeolitic units were functionalized using 8 mol% of PHAPTMS (with respect to  
2 the silica content in the initial gel), and the silanization reaction was performed at 90 °C for 6 h,  
3 under reflux, followed by crystallisation at 170 °C for 184-186 h in a PTFE-lined stainless-steel  
4 autoclave, under static, hydrothermal conditions. After cooling, the resultant product was recovered  
5 by centrifugation, washed thoroughly with milliQ-water and dried at 110 °C overnight. The solid  
6 was gently grinded using an Agate mortar and pestle, and calcined at 550 °C in static air for 5 h  
7 (heating rate of 1 °C min<sup>-1</sup>), giving a material denoted hZSM-5(x)-PZSi (PZSi stands for  
8 ProtoZeolitic units subjected to Silanization), where x stands for the Si/Al ratio of the synthesis gel.  
9 The resulting hZSM-5(51)-PZSi material was submitted to a mesopore narrowing treatment.  
10 Specifically, 1.0 g of material was dispersed in 62.8 g of a 0.37 M NH<sub>4</sub>OH aqueous solution  
11 containing 0.7 g of CTAB. The resulting mixture was stirred at room temperature for 30 min, and  
12 then subjected to a hydrothermal treatment under static conditions, for 20 h at 150 °C in a PTFE-  
13 lined stainless-steel autoclave. The resultant product was recovered by centrifugation, washed  
14 thoroughly with milliQ-water and dried at 110 °C overnight. The solid was gently grinded using an  
15 Agate mortar and pestle, and calcined at 550 °C in static air for 5 h (heating rate of 1 °C min<sup>-1</sup>),  
16 giving a material denoted hZSM-5(47)-PZSiS (PZSiS stands for ProtoZeolitic units subjected to  
17 Silanization, followed by Surfactant treatment). This protocol does not require ion-exchange since no  
18 alkaline source is used.

19

### 20 2.2.3. Sample hZSM-5(31)-CoT

21 The co-templating method was carried out following a similar procedure to that described by Wang  
22 et al. [44]. Specifically, 0.43 mmol of NaAlO<sub>2</sub>, 9.8 mmol of TPAOH and 31.0 mmol of TEOS were  
23 mixed with 1268 mmol of milliQ-water under stirring and aged at 100 °C for 3 h. Then, 3.0 mmol of  
24 PDD-AM were added into the reaction mixture. The molar composition of the synthesis-gel was  
25 1Al<sub>2</sub>O<sub>3</sub>: 72SiO<sub>2</sub>: 1.3 Na<sub>2</sub>O: 23TPAOH: 4000 H<sub>2</sub>O. The mixture was stirred for 15-16 h at room

1 temperature, and then was transferred into a PTFE-lined stainless-steel autoclave for crystallization  
2 at 180 °C for 144 h. The resulting product was collected by centrifugation, washed thoroughly with  
3 milliQ-water and dried at 100 °C overnight. The solid was gently grinded using an Agate mortar and  
4 pestle, and calcined at 550 °C in static air for 5 h (heating rate of 1 °C min<sup>-1</sup>). The protonic form was  
5 obtained by ion-exchange with 1.0 M NH<sub>4</sub>NO<sub>3</sub> aqueous solution (1 g of calcined sample per 10 mL  
6 of solution), at 80 °C, under stirring. The solution was renewed three times, every 2 h. Finally, the  
7 solid was centrifuged, washed with milliQ water, dried at 100 °C over-night, and calcined at 550 °C  
8 in static air for 4 h (heating rate of 1 °C min<sup>-1</sup>), giving a material denoted hZSM-5(31)-CoT (CoT  
9 stands for co-template).

10  
11 ((Table 1 here))

### 12 13 **2.3. Characterisation of the catalysts**

14 The PXRD data were collected on an Empyrean PANalytical diffractometer (Cu<sub>Kα</sub> X-radiation,  
15  $\lambda=1.54060$  Å) in a Bragg-Brentano para-focusing optics configuration (45 kV, 40 mA). Samples  
16 were prepared in a spinning flat plate sample holder and step-scanned in the range from 3 to 70° ( $2\theta$ )  
17 with steps of 0.026°. A PIXEL linear detector with an active area of 1.7462° was used with a  
18 counting time of 68 s per step. The low angle (0.5-5°  $2\theta$ ) PXRD data were collected using the  
19 transmission mode, and with the sample deposited between Mylar foils; the samples were step-  
20 scanned in 0.01°  $2\theta$  steps with a counting time of 80 s per linear detector active area of 2.0°.

21 SEM images, EDS analysis and elemental mappings (Al, Si) were obtained on a Hitachi SU-70 SEM  
22 microscope with a Bruker Quantax 400 detector operating at 20 kV. TEM was performed on a  
23 Hitachi HD2700 instrument, and the samples were prepared by spotting carbon-film-coated 400  
24 mesh copper grids (Agar Scientific) with a suspension of the solid sample in ethanol.

1 Nitrogen adsorption-desorption isotherms were measured at 196 °C, using a Quantachrome  
2 instrument (automated gas sorption data using Autosorb IQ<sub>2</sub>). The samples were pre-treated at 300  
3 °C for 3 h, under vacuum (3 Torr). The external or mesopore surface area ( $S_{ext,meso}$ ) and micropore  
4 volume ( $V_{micro}$ ), were calculated by the t-plot method. The pore size distributions ( $D_p$ ) were  
5 determined by the DFT method (adsorption branch). Differential scanning calorimetry analyses  
6 (DSC) were performed under air, from room temperature until 800 °C, with a heating rate of 10 °C  
7  $min^{-1}$ , using a Shimadzu DSC-50 instrument.

8 The  $^{27}Al$  MAS NMR spectra were recorded at 182.432 MHz using a Bruker Avance 700 (16.4 T)  
9 spectrometer with a unique pulse, a recycle delay of 1 s and a spinning rate of 14 kHz. The acid  
10 properties were measured using a NexusThermo Nicolet apparatus (64 scans and resolution of 4  $cm^{-1}$   
11  $^1$ ) equipped with a home-made vacuum cell, using self-supported discs (5-10  $mg\ cm^{-2}$ ) and pyridine  
12 as the basic probe. After in situ outgassing at 450 °C for 3 h ( $10^{-6}$  mbar), pyridine (99.99 %) was  
13 contacted with the sample at 200 °C for 10 min and subsequently evacuated at the same temperature  
14 or at 450 °C for 30 min, under vacuum ( $10^{-6}$  mbar). The IR bands at  $\approx 1540$  and  $1455\ cm^{-1}$ , which are  
15 related to pyridine adsorbed on Brønsted (B) and Lewis (L) acid sites, respectively, were used for  
16 quantification [50]. The total amount of acid sites (L+B) and the molar ratios L/B were determined at  
17 the lowest desorption temperature (200 °C). The amount of strong acid sites was evaluated by the  
18 molar ratios  $B_{450}/B_{200}$  (B acid strength) and  $L_{450}/L_{200}$  (L acid strength), respectively, where  $L_T$  and  $B_T$   
19 are the amount of L and B acid sites, respectively, which remained in the solid material after  
20 evacuation at  $T=450$  or 200 °C.

#### 21 22 **2.4. Catalytic tests**

23 The catalytic oligomerisation of 1-butene (1C<sub>4</sub>) was carried out under continuous-flow, high-pressure  
24 conditions, using a stainless steel, fixed-bed reactor (10 mm internal diameter). A simplified  
25 representation of the experimental setup is given in Figure 1, indicating the equipment used for

controlling the feed flow rate (for 1C<sub>4</sub>, a syringe pump Chemyx, model Nexus 6000; and for N<sub>2</sub>, a gas mass flow controller Bronkhorst, EL-FLOW), pressure (backpressure regulator located after the reactor; Equilibar, LF-Primary Research Series) and temperature (furnace (Termolab), temperature controller and thermocouple located inside the reactor). The reactor was loaded with catalyst (150 mg) and silicon carbide (diluent to enable a uniform temperature distribution along the catalytic bed); the total bed volume was  $\approx 1.8 \text{ cm}^3$ . The catalysts were activated at 450 °C for 3 h under nitrogen flow ( $10 \text{ cm}^3 \text{ min}^{-1}$ ) prior to the catalytic reaction. Subsequently, the reactor temperature was set to the desired catalytic reaction temperature, and the olefin was fed using nitrogen as the carrier gas (molar ratio of 1C<sub>4</sub>:N<sub>2</sub> = 15:85).

((Figure 1 here))

The gas phase (non-condensed compounds) was sampled in regular intervals of  $\approx 1 \text{ h}$ , for a time-on-stream (TOS) of  $\approx 7 \text{ h}$ , using loops (heated at 200 °C) which were connected on-line to the Master Fast GC gas chromatography instrument (DANI) equipped with a capillary column (ValcoBond VB-1, 60 m x 0.25 mm x 1.50  $\mu\text{m}$ ), FID detector, and a split/splitless injector. Quantifications were based on external calibration curves using pure 1C<sub>4</sub>; the experimental range of error was less than 5 %. The catalytic results were expressed as conversion of butenes ( $X_{C_4}$ ) which did not react to give higher molar mass products using the equation  $X_{C_4} (\%) = \frac{F_{1C_4in} - F_{C_4out}}{F_{1C_4in}} \times 100$ , where  $F_{1C_4in}$  is the inlet molar flow rate of 1-butene, and  $F_{C_4out}$  is the outlet molar flow rate of butenes. The values of  $X_{C_4}$  correspond to the conversion at  $\approx 7 \text{ h}$  on-stream, excluding the values presented as a function of TOS where  $X_{C_4}$  is calculated for each point (Figure S5).

The liquid reaction products were condensed in a jacketed cooling trap (cooling fluid at 5 °C; pressure inside the trap was  $\approx 1 \text{ bar}$ ), and the mixture was analysed using the same GC instrument; concentrations were based on calibrations using ASTM D2887 Quantitative Calibration mixture (*n*-

1 alkanes C<sub>6</sub>-C<sub>44</sub>), and internal standard. The products lump distributions (PLD) curves correspond to  
2 the products formed during ≈7 h TOS. These curves are represent the set of values of selectivity  
3 (S<sub>C<sub>[y-z]</sub></sub>) towards a lump of compounds possessing y to z number of carbon atoms per molecule (lump  
4 C<sub>[y-z]</sub>, where z > y), which was calculated using the equation  $S_{C_{[y-z]}} (\%) = \frac{n_{C_{[y-z]}}}{\sum n_{C_{[y-z]}}} \times 10$ , where  $n_{C_{[y-z]}}$   
5 is the moles for product lump C<sub>[y-z]</sub> multiplied by [(y+z)/2], and  $\sum n_{C_{[y-z]}}$  is the total moles of products  
6 in the range C<sub>6</sub>-C<sub>24</sub>. The fractions corresponding to the 170 °C cut characteristic of naphtha products  
7 (NCut), and to the 170-390 °C cut characteristic of diesel products (DCut, corresponding  
8 approximately to the C<sub>10</sub>-C<sub>24</sub> n-paraffinic range) were determined according to the ASTM D2887  
9 method (Standard Test Method for Boiling Range Distribution of Petroleum Fractions by Gas  
10 Chromatography) [37,43,51]. These analyses were validated using the ASTM D2887 Reference Gas  
11 Oil n.º 1 (Supelco, sample 1, Batch 2) and the results agreed, within the allowable difference ranges,  
12 with the ASTM D2887 consensus boiling point values. It is worth mentioning that C<sub>10</sub> type products  
13 (based on the temperature cut point) may be distributed between the DCut and NCut fractions. The  
14 average space time yields (STY, expressed as mg g<sub>cat</sub><sup>-1</sup> h<sup>-1</sup>) were based on the mass fractions of DCut  
15 and NCut of total liquid (condensed) products formed during ≈7 h TOS. In general, the material  
16 balances closed in at least 85 %. The catalytic performances were compared based on X<sub>C4</sub> and STYs  
17 considering approximately steady-state conditions within ≈7 h TOS.

18 The spent catalysts were thermally treated at 550 °C (1 °C min<sup>-1</sup>) for 6 h, to burn-off carbonaceous  
19 matter, giving the recovered solids, which were characterised or used for catalytic tests. Details  
20 regarding the determination of the cetane number (CN, based on <sup>1</sup>H NMR spectroscopy),  
21 isoparaffinic index (I, based on <sup>1</sup>H NMR spectroscopy), aromatics content (%Ar, based on <sup>1</sup>H NMR  
22 spectroscopy) of the reaction products, the amount of coke (based on elemental analysis) present in  
23 the spent catalysts, and checking for operation under kinetic regime, are given in the Supplementary  
24 Material.

25

### 3. Results and Discussion

#### 3.1. Characterisation of the catalysts

Micro/mesoporous materials based on the MFI topology were prepared via bottom-up approaches, under hydrothermal conditions. The MFI features of the materials prepared were ascertained by PXRD diffraction, which showed the characteristic reflections in the range  $7-57^\circ 2\theta$ , with the most intense peaks at  $7-8^\circ$  and  $23-24^\circ 2\theta$  (Figure 2) [52,53]. Low angle PXRD showed a broad peak in the range  $0.5-1.5^\circ 2\theta$ , likely associated with the mesoporous features of the zeotypes prepared (Figure S1).

((Figure 2 here))

Figure 3 shows the SEM and STEM images of the zeotypes. The noT and the PZSi(S) protocols led to materials consisting of pseudo-spherical aggregates ( $\approx 200-400$  nm in size, Figure 3-a,d,g,j) of nanocrystallites ( $\approx 10-60$  nm, Figure 3-c,f,i,l), somewhat in agreement with literature data for similarly prepared materials [46,49]. The PZSiS protocol involving a final surfactant treatment seemed to lead to some coalescence (Figures 3-k), forming larger nanocrystallites of  $\approx 30-60$  nm compared to  $\approx 10-20$  nm for PZSi. The CoT protocol led to irregular aggregates (ca.  $1-1.5 \mu\text{m}$ ) of nanocrystallites ( $\approx 30-40$  nm), Figure 3-m,n,o. Commercial ZSM-5 zeolite (ZSM-5(29)) consists of small microcrystals ( $100-300$  nm, Figure 3-p,q,r). EDS (Table 2) and Si and Al mappings (Figure S2) suggested that the materials possessed uniform dispersions of metal/metalloid surface species, and the molar ratios Si/Al were in the range 20-51 (Table 2).

((Figure 3 and Table 2 here))

1 The materials possessed BET specific surface area ( $S_{\text{BET}}$ ) in the range 308-853  $\text{m}^2\text{g}^{-1}$  (Table 2), and  
2 both micro- and mesoporosity (micropore sizes of 0.55-0.57 nm, and mesopore sizes of 2-10 nm,  
3 Figure 4). For the prepared zeotypes excluding hZSM-5(31)-CoT, the portion of specific mesopore  
4 surface area ( $S_{\text{meso}}$ ) was in the range 43-59 %, and that of micropore volume was 7-12 %. The  
5 material hZSM-5(31)-CoT possessed highest  $S_{\text{BET}}$  (853  $\text{m}^2\text{g}^{-1}$ ), albeit the portion of microporous  
6 volume was considerable (52 %). The commercial zeolite ZSM-5(29) possessed the lowest  $S_{\text{meso}}$ .

7  
8 ((Figure 4 here))

9  
10 FT-IR spectroscopy of the dehydrated materials (self-supported samples) showed a band centered at  
11 ca. 3743  $\text{cm}^{-1}$ , and a shoulder at ca. 3730  $\text{cm}^{-1}$ , which seemed more pronounced for the zeotypes than  
12 zeolite ZSM-5(29) (Figure S3-A). The band at ca. 3743  $\text{cm}^{-1}$  is assignable to the OH stretching  
13 vibration of isolated silanol groups, and that at ca. 3730  $\text{cm}^{-1}$  may be due to weakly perturbed silanol  
14 groups (e.g. defect sites) [54,55].

15 The materials were characterised at the molecular level by  $^{27}\text{Al}$  MAS NMR spectroscopy to identify  
16 the types of Al species, and FT-IR spectroscopy using pyridine as base probe to investigate the  
17 surface acidity.  $^{27}\text{Al}$  MAS NMR spectroscopy indicated that all materials exhibited a main resonance  
18 centered at ca. 55 ppm assignable to four-coordinated (framework) aluminum species ( $\text{Al}_{\text{tetra}}$ ), and a  
19 small resonance at ca. 0 ppm assignable to six-coordinated Al species ( $\text{Al}_{\text{octa}}$ ) which may be bonded  
20 or not to the framework (Figure S4, Table 3) [56]. The ratio  $\text{Al}_{\text{tetra}}/\text{Al}_{\text{octa}}$  (determined via  
21 deconvolution of the spectra and integration of the peaks) were in the range 3-13 for the zeotypes  
22 and 16 for zeolite ZSM-5(29). The lower  $\text{Al}_{\text{tetra}}/\text{Al}_{\text{octa}}$  together with the above FT-IR spectroscopic  
23 results for the zeotypes, suggest that these may possess more defect sites than the zeolite, which may  
24 be partly associated with the reduced crystallite sizes of the zeotypes.

1 The acid properties measured by FT-IR spectroscopy of adsorbed pyridine (base probe) are indicated  
2 in Table 3. All materials exhibited bands at  $\approx 1540$  and  $1455\text{ cm}^{-1}$  assigned to Brønsted and Lewis  
3 acid sites (Figure S3-B) [50]. In general, the zeotypes and zeolite ZSM5(29) possessed essentially  
4 strong Lewis acid sites ( $L_{450}/L_{200}$  in the range  $\sim 0.5-1$ ) and weak/moderate Brønsted acidity ( $B_{450}/B_{200}$   
5  $< 0.3$ ) (Table 3). Zeolite ZSM-5(29) possessed the higher amount of total acid sites (L+B) than the  
6 zeotypes. Of the zeotypes, hZSM-5(31)-noT and hZSM-5(20)-PZSi possessed highest (and similar)  
7 L+B ( $251-252\text{ }\mu\text{mol g}^{-1}$ ). The noT and CoT protocols gave materials possessing comparable or  
8 stronger acidity to zeolite ZSM-5(29), whereas the PZSi protocol gave materials possessing weaker  
9 acidity. Changing the Si/Al ratio of the materials prepared via the PZSi protocol influenced L+B and  
10 the molar ratio L/B, without affecting significantly the acid strength; L+B and L/B increased with  
11 decreasing Si/Al ratio (Table 3). The zeotype hZSM-5(20)-PZSi possessed the highest molar ratio  
12 L/B of 1.3, compared to  $< 0.6$  for the remaining materials.

13

14 ((Table 3 here))

15

## 16 **3.2. Catalytic oligomerisation**

### 17 3.2.1. General considerations

18 The MFI-based materials prepared via the bottom-up synthetic approaches were tested for the  
19 oligomerisation of 1-butene (1C4), under high-pressure (30 bar) continuous-flow conditions, at 200  
20 °C, and weight hourly space velocity (WHSV) of  $2.2\text{ g}_{1\text{C}4}\text{ g}_{\text{cat}}^{-1}\text{ h}^{-1}$ . Previous studies using Beta type  
21 catalysts (and the same reactor setup) indicated that these conditions were a reasonable compromise  
22 for targeting diesel cut products with low aromatics content, operating under kinetic regime [57].  
23 WHSV of  $2.2\text{ g}_{1\text{C}4}\text{ g}_{\text{cat}}^{-1}\text{ h}^{-1}$  somewhat lies in the range of values of WHSV for olefin oligomerisation  
24 technologies such as, Mobil Olefins to Gasoline and Distillate (MOGD; WHSV of  $0.5-2\text{ h}^{-1}$  [58,59]).  
25 All materials prepared were effective in converting 1-butene (1C4) to higher molar mass products.



1 The gaseous effluent stream contained essentially unreacted 1C4 and its isomers cis-2-butene and  
2 trans-2-butene. The conversion of total butenes ( $X_{C4}$ ) was in the range 27-77 % (Figure 5). For all  
3 catalysts, the molar ratio of (C4 isomer products):1C4 was in the range 5.0-5.7, and the ratio of  
4 cis:trans isomers was ca. 0.6. The predominance of the trans C4 isomer is in agreement with  
5 literature data for the isomerization of 1C4 [60]. The isomer distributions with chains of a given size  
6 may be independent of the type of solid acid catalyst, and correspond to thermodynamic equilibrium  
7 compositions [61]. On the other hand, alkenes possessing terminal C=C bonds may undergo faster  
8 oligomerisation than alkenes possessing internal C=C bonds [62,63], contributing to the  
9 predominance of the internal C4 isomers over 1C4.

10 The liquid product lump distribution (PLD) curves corresponded products possessing number of  
11 carbon atoms in the range C6-C24, i.e. products with boiling point ranges corresponding to the 170  
12 °C cut (C<sub>6</sub>-C<sub>10</sub>) characteristic of naphtha type products (NCut), and the 170-390 °C cut (C<sub>10</sub>-C<sub>24</sub>)  
13 characteristic of diesel type products (DCut) (Figure 6). A comparative study for all materials,  
14 indicated that the zeotypes possessed different catalytic activity and led to different average space-  
15 time yields of liquid products (STY). Higher catalytic activity seemed accompanied by a greater  
16 production of higher molar mass products (Figure 7). In general, the zeotypes performed superiorly  
17 to commercial zeolite ZSM-5(29) ( $X_{C4} = 27\%$ ,  $STY = 58\text{ mg g}_{\text{cat}}^{-1}\text{ h}^{-1}$ , Figure 5). The best-  
18 performing zeotype was hZSM-5(20)-PZSi, which led to  $X_{C4} = 77\%$  and  $STY = 791\text{ mg g}_{\text{cat}}^{-1}\text{ h}^{-1}$ ,  
19 with the predominance of DCut products (mass ratio of DCut:NCut = 2.1 and  $STY_{\text{DCut}} = 534\text{ mg g}_{\text{cat}}^{-1}$   
20  $\text{h}^{-1}$ , TOS = 7 h).

21 The overall reaction mechanism of these systems may be very complex, involving for example,  
22 primary/secondary cracking and alkylation reactions, besides isomerisation (e.g. double bond or  
23 methyl shifts) and oligomerisation [64]. The relative amount of aromatic products ( $H_{\text{ar}}$ ) and the  
24 isoparaffinic ratio ( $I$ ), which reflects the degree of branching of the liquid products, were determined  
25 by <sup>1</sup>H NMR spectroscopic analysis of the liquid reaction products (details in the Supplementary

1 Material). For all materials,  $H_{ar} < 0.2$  %, indicating very low aromatics content. The low aromatics  
2 content and the absence of heteroatoms are advantages of light olefin oligomerisation routes for  
3 synthesising clean fuels. The  $I$  values were in the range 0.47-0.59, based on the O'Connor or Kapur  
4 methods [65,66]. These results are advantageously lower than that reported in the literature for a  
5 mesostructured zeotype based on the BEA topology ( $I \approx 0.62$ ) [57], tested under similar 1C4 reaction  
6 conditions. An estimation of the cetane number (CN, based on the O'Connor method [65]) indicated  
7 values in the range 43-50 (noteworthy, without post-treatments such as hydrogenation that increase  
8 the CN [67]). Literature data for CN of diesel cuts produced in commercial processes, and  
9 commercial diesel samples were in the range 48-56 [28,66,68-70].

10  
11 ((Figures 5 and 6 here)))

12  
13 The most active catalyst hZSM-5(20)-PZSi was further tested under different reaction conditions  
14 (Table 4). The catalyst activation temperature ( $T_{act}$ ) of 200 °C or 450 °C prior to the oligomerisation  
15 reaction led to comparable catalytic results (similar  $X_{C4}$  and STY at 200 °C, 30 bar). Different results  
16 were reported in the literature for micro-mesoporous zeotypes based on the BEA topology, for which  
17 higher  $T_{act}$  led to poorer catalytic results;  $T_{act}$  may affect the coordination environment (and  
18 configuration) of the Al species of the BEA framework [57]. Conversion and STY increased with  
19 increasing reaction temperature from 200 to 250 °C, whereas the mass ratio DCut/NCut decreased  
20 from 2.1 to 1.5. Hence, while the total productivity may be favoured by increasing the temperature,  
21 albeit the relative amount of DCut products decreases, which is consistent with the fact that the  
22 oligomerisation reaction is exothermic. Increasing the reaction pressure from 30 to 40 bar led to  
23 enhanced  $X_{C4}$  (87 and 97 %, respectively) and  $STY_{DCut}$  (611 and 669  $mg\ g_{cat}^{-1}\ h^{-1}$ , respectively) at  
24 250 °C. These results are consistent with the fact that oligomerisation leads to reduction in the total  
25 number of molecules in the reaction system, and thus may be favored with increased pressure.

1  
2  
3  
4  
5  
6  
7  
8  
9  
10  
11  
12  
13  
14  
15  
16  
17  
18  
19  
20  
21  
22  
23  
24  
25

((Figure 7 and Table 4 here))

The results for the best-performing catalyst hZSM-5(20)-PZSi ( $X_{C_4} = 77\%$ ,  $STY = 791 \text{ mg g}_{\text{cat}}^{-1} \text{ h}^{-1}$ , mass ratio DCut/NCut = 2.1) compare favourably to literature data for several types of aluminosilicates, tested under similar 1C4 reaction conditions (200 °C, 30 bar): mesoporous aluminosilicates possessing amorphous pore walls [24]; versions of (large-pore) zeolite Beta such as, microcrystalline or nanocrystalline zeolite Beta [57]; and a composite of BEA nanocrystals embedded in a mesoporous siliceous matrix (Table S1) [57]. Interesting results were reported for a hierarchical zeotype based on the BEA topology ( $T_{\text{act}} = 200 \text{ °C}$ ) which led to  $X_{C_4}$  (54 %), and STY of  $502 \text{ mg g}_{\text{cat}}^{-1} \text{ h}^{-1}$ , and commercial zeolite ZSM-5 with Si/Al = 15 ( $T_{\text{act}} = 450 \text{ °C}$ ) which led to  $X_{C_4} = 39\%$  and  $STY = 523 \text{ mg g}_{\text{cat}}^{-1} \text{ h}^{-1}$  [24,57]. Several studies reported 1C4 conversion over commercial ZSM-5, under different reaction conditions; one of the best results in terms of selectivity to diesel products was reported by Schwarz et al. [71], specifically, 76 wt% diesel selectivity at 99 % 1C4 conversion (conversion of total butenes not specified), at 270 °C, 50 bar (Table S1). Under roughly comparable temperature and pressure conditions to those used by Schwarz et al., Li et al. [72] reported the conversion of butene (isomer not specified), over a ZSM-5 type material synthesised hydrothermally using hemicellulose, the initiator ammonium persulphate and tetramethylethylenediamine, which led to 88 % diesel selectivity at 91 % conversion, 40 bar, 270 °C ( $WHSV = 4.8 \text{ g}_{1C_4} \text{ g}_{\text{cat}}^{-1} \text{ h}^{-1}$ ) (Table S1); this material possessed 17 %  $S_{\text{meso}}$  and 33 %  $V_{\text{micro}}$  compared to 13 %  $S_{\text{meso}}$  and 38 %  $V_{\text{micro}}$  for ZSM-5 prepared in a conventional fashion, which together with the higher amount of total acid sites of the former, led to improved catalytic performance in relation to the conventional zeolite [72].

### 3.2.2. Influence of material properties

1 Conversion followed the order ( $X_{C_4}$ ): hZSM-5(31)-CoT (27 %)  $\approx$  hZSM-5(47)-PZSiS (28 %) <  
2 hZSM-5(31)-noT (54 %)  $\approx$  hZSM-5(51)-PZSi (57 %) < hZSM-5(20)-PZSi (77 %). On the other  
3 hand, the total STY followed the order ( $\text{mg g}_{\text{cat}}^{-1} \text{h}^{-1}$ ): hZSM-5(31)-CoT (43) < hZSM-5(47)-PZSiS  
4 (235) < hZSM-5(51)-PZSi (496) < hZSM-5(31)-noT (521) < hZSM-5(20)-PZSi (791). Direct  
5 relationships between the catalytic activity and the textural or acid properties could not be clearly  
6 established considering all materials at once. The catalytic performance may result from complex  
7 interplay of several properties including morphology, texture and acidity, which, in turn, depend on  
8 the synthesis protocol. It is important to reduce the number of variables in comparative studies to  
9 gain insights into structure-activity relationships. The materials prepared via the protocols CoT and  
10 noT possess the same molar ratio Si/Al (31) and roughly comparable  $S_{\text{meso}}$  (140 and 168  $\text{m}^2 \text{g}^{-1}$ ,  
11 respectively), Table 3. Yet, their catalytic performances were very different, with hZSM-5(31)-noT  
12 performing far superiorly to hZSM-5(31)-CoT;  $X_{C_4}$  of 54 and 27 %, and STY of 522 and 43  $\text{mg g}_{\text{cat}}^{-1}$   
13  $\text{h}^{-1}$ , respectively. Zeotype hZSM-5(31)-noT possessed more regular morphology (Figure 3), lower  
14  $V_{\text{micro}}$  and higher amount of acid sites (Table 3) than hZSM-5(31)-CoT, which may result in a higher  
15 amount of effective (accessible) active sites in the former case, favouring the oligomerisation  
16 reaction.

17 Zeolite ZSM-5(29) possessed highest amount of acid sites, albeit its catalytic activity was similar to  
18 the least active material prepared namely hZSM-5(31)-CoT. The larger crystallite sizes (micron  
19 range) and relatively low  $S_{\text{meso}}$  of ZSM-5(29) may account for longer diffusional pathways and  
20 important steric hindrance effects. Hence, nanocrystals, mesoporosity and regular morphology seem  
21 important features to meet superior catalytic performances.

22 The materials based on the PZSi synthetic approach were consisted of pseudo-spherical aggregates  
23 of nanocrystallites of 10-60 nm in size, and possessed comparable  $V_p$ ,  $V_{\text{micro}}$  and  $S_{\text{meso}}$  (275-308  $\text{m}^2$   
24  $\text{g}^{-1}$ ) and acid strengths. However, their catalytic performances were different, which seemed to be  
25 related to the relative amount of Lewis acid sites. Specifically,  $X_{C_4}$  and STY increased with L/B,

1 being highest for hZSM-5(20)-PZSi (Figure 8). Thus, the Lewis acidity seems favourable for the  
2 catalytic reaction. These results are in agreement with literature data for the oligomerisation of C4  
3 olefins; e.g. 1C4 conversion over zeotypes possessing BEA topology [57], and isobutene conversion  
4 over commercial zeolite Beta [73], dealuminated zeolite Y or zeolite Y-supported AlCl<sub>3</sub> [42,74].  
5 Since the material properties requirements may be different for olefins of different carbon chain  
6 lengths [37], comparisons have been restricted to C4 olefins. The post-synthesis surfactant treatment  
7 of hZSM-5(51)-PZSi gave hZSM-5(47)-PZSiS, which did not lead to improved X<sub>C4</sub> or STY (Figure  
8 5); these results may be partly due to the lower L/B of hZSM-5(47)-PZSiS (Table 3).

9 Overall, the noT and PZSi synthetic strategies seem promising for preparing zeotype catalysts for  
10 olefin oligomerisation. One of the parameters that may be varied in all synthesis protocols is the  
11 Si/Al ratio, which may influence the acid properties of the final materials. The material prepared via  
12 the noT protocol (Si/Al = 31) possessed intermediate Si/Al ratio of the two PZSi based materials (20-  
13 51). Nevertheless, hZSM-5(31)-noT resembled somewhat closely the catalytic performance of  
14 hZSM-5(51)-PZSi and was outperformed by hZSM-5(20)-PZSi. The PZSi protocol seems to  
15 advantageously give materials with enhanced L/B ratio and S<sub>meso</sub> for butene oligomerisation.

16  
17 ((Figure 8 here))

### 18 19 3.2.3. Catalytic stability

20  
21 The catalyst stabilities of hZSM-5(20)-PZSi and hZSM-5(51)-PZSi were investigated, and compared  
22 to zeolite ZSM-5(29), at 200 °C, 30 bar. The originally pristine white solid catalysts turned brown in  
23 colour after the catalytic reaction. The carbon content of the washed/dried catalysts was ca. 13 wt%  
24 C (based on elemental analysis). DSC analysis of the used catalysts under air atmosphere indicated  
25 an endothermic process occurring at temperature lower than 200 °C, which was likely the desorption

1 of physisorbed water and other volatiles (exemplified for hZSM-5(20)-PZSi in Figure S6).  
2 Additionally, an exothermic process with an onset at ca. 280 °C occurred for the used catalysts, but  
3 not for the unused ones. The exothermic process was likely the combustion of coke deposits. The  
4 catalysts were regenerated by the thermal treatment at 550 °C and turned off-white in colour,  
5 suggesting that most of the coke was removed.

6 The regenerated catalysts were characterized in what regards the morphology (SEM, TEM),  
7 composition (EDS), crystal structure (PXRD), textural properties (N<sub>2</sub> adsorption), surface Al species  
8 (<sup>27</sup>Al MAS NMR) and acid properties (FT-IR spectroscopy of adsorbed pyridine). For the three  
9 catalysts, the MFI crystalline structure was essentially preserved during the catalytic process (Figure  
10 9), and the morphology (Figure S7) and textural properties remained similar (Table S2). For the  
11 zeotypes, the Si/Al ratio remained roughly constant, and molecular level characterization studies  
12 indicated the predominance of Al<sub>tetra</sub> species and comparable L/B ratio (Table S3). The most  
13 pronounced difference was slight decrease of L+B for the used catalyst hZSM-5(20)-PZSi. The  
14 commercial zeolite ZSM-5(29) suffered drop in the Si/Al ratio, %Al<sub>tetra</sub> and L+B, which was  
15 accompanied by the appearance of five-coordinated Al species (band at ca. 25 ppm due to Al<sub>penta</sub>)  
16 and slight increase in L/B. Based on the results regarding the material properties, the zeotypes  
17 seemed more stable than the zeolite.

18  
19 ((Figure 9 here))

20  
21 The catalysts were used for two consecutive 7 h-on stream cycles, with an intermediate step of  
22 catalyst regeneration. From the first to the second cycle it was verified partial catalyst deactivation,  
23 which was more pronounced for the zeotypes (X<sub>C4</sub> at TOS=7 h decreased by a factor of ca. 1.44)  
24 than ZSM-5(29) (X<sub>C4</sub> decreased by a factor of ca. 1.4) (Figure 10). The drop in activity of ZSM-  
25 5(29) somewhat correlates with the changes in surface Al<sub>tetra</sub> species and acid properties of the use

1 catalyst (discussed above). For the zeotypes, the partial catalyst deactivation does not correlate with  
2 the characterization results, which indicated that the physicochemical properties of the materials  
3 were fairly well preserved, especially in the case of hZSM-5(51)-PZSi.

4 The MFI based materials possess crystallographically different Al species, for which the intrinsic  
5 activity and stability may be different. Molecular-level changes may occur during the catalytic  
6 process, which are difficult to track by the characterization studies of the solids recovered after the  
7 catalytic reaction. Although the original and used zeotypes exhibited similar  $^{27}\text{Al}$  MAS NMR  
8 spectra, it is important to consider that there may exist “NMR-invisible” Al species [75-77]. Woolery  
9 et al. [56] reported for MFI zeolites that treatment at high temperature may lead to the hydrolysis of  
10 Al-O bonds (e.g. less stable Al species subjected to local stress in a confined environment) and the  
11 formation of “NMR-invisible” Al species of Lewis type. The extent of the hydrolysis of the  
12 framework species may increase with temperature [75]. Accordingly, the reaction conditions and the  
13 temperature distribution along the catalytic bed may affect the catalyst stability. The  $\text{Al}_{\text{tetra}}$  species  
14 may undergo hydrolysis to give framework-bonded  $\text{Al}_{\text{octa}}$  species; the latter may react reversibly to  
15 give  $\text{Al}_{\text{tetra}}$  species by the interaction with base molecules such as pyridine [75], which was used as  
16 probe for measuring the acid properties. Hence, although the molecular-level characterisation studies  
17 based on the spectroscopic techniques  $^{27}\text{Al}$  MAS NMR and FT-IR of adsorbed pyridine gave similar  
18 results for the original and used hZSM-5(51)-PZSi catalysts, for example, this does not rule out the  
19 possibility of occurring in situ changes of surface species; it is not trivial to track these possible  
20 modifications, and assess the intrinsic activities and relative amounts of the in situ modified surface  
21 species in order to study their influence on the catalytic reaction.

22  
23 ((Figure 10 here))

#### 24 25 **4. Conclusions**

1 Non-destructive bottom-up synthetic approaches led to MFI-based zeotype catalysts with favourable  
2 morphological, textural and acid properties for olefin oligomerisation to higher molar mass products,  
3 under high-pressure continuous-flow conditions. In general, the zeotypes consisting of  
4 morphologically regular aggregates of nanocrystallites and possessing mesoporosity outperformed  
5 microcrystalline zeolite ZSM-5 in 1-butene oligomerisation, at 200 °C, 30 bar (even though the  
6 zeolite possessed the highest amount of total acid sites). The best performing zeotype was hZSM-  
7 5(20)-PZSi (Si/Al = 20), prepared via the Serrano et al. [46-48] strategy (PZSi) based on the  
8 crystallization of silanized protozeolitic units; 77 % conversion of butenes, average space time yield  
9 of liquid products of  $791 \text{ mg g}_{\text{cat}}^{-1} \text{ h}^{-1}$  (7 h on-stream) and mass ratio DCut/NCut = 2. These results  
10 compared favourably to literature data for several aluminosilicates tested under similar 1-butene  
11 oligomerisation reaction conditions. The materials prepared via the PZSi approach seemed to benefit  
12 from enhanced mesoporosity and L/B ratio for butene oligomerisation.

13 Characterization studies indicated that the morphology, structure, composition, textural and acid  
14 properties of the zeotypes were essentially preserved during the catalytic reaction and the catalyst  
15 regeneration processes. Molecular-level characterization of the zeotypes and the zeolite, suggested  
16 superior stability of the former in what concerns the Al-species and acid properties. However, partial  
17 drop in catalytic activity was verified for the regenerated catalysts, possibly due to changes in surface  
18 chemical properties occurring in situ, under the operating conditions. It is not trivial to track these  
19 changes by characterisation studies of the catalysts recovered after the reaction. While envisaging  
20 zeotypes as promising catalysts for olefin oligomerisation, important future challenges include in situ  
21 high temperature characterisation studies to track possible changes in surface chemical species  
22 occurring under the operating conditions, and gain more insights into effective structure-activity  
23 relationships, which may aid in the improvement of material properties to meet superior  
24 performances.

25



## 1 Acknowledgements

2 This work was developed in the scope of the project (Associate Laboratory) CICECO Aveiro  
3 Institute of Materials-POCI-01-0145-FEDER-007679 [FCT (Fundação para a Ciência e a  
4 Tecnologia) ref. UID/CTM/50011/2013], and QOPNA research Unit (FCT UID/QUI/00062/2013),  
5 financed by national funds through the FCT/MEC and when applicable co-financed by FEDER  
6 (Fundo Europeu de Desenvolvimento Regional) under the PT2020 Partnership Agreement. The FCT  
7 and the European Union are acknowledged for a Ph.D. grant to A.F.S. (SFRH/BD/101018/2014),  
8 and post-doctoral grants to A.F (SFRH/BPD/91397/2012) and M.A. (SFRH/BPD/89068/2012), co-  
9 funded by MCTES and the European Social Fund through the program POPH of QREN. The authors  
10 wish to thank Saint-Gobain Ceramic Materials AS for generously supplying the SIKA SiC sample.

## 12 References

- 13 [1] U.S. Administration Energy Information. International Energy Outlook 2016,  
14 [https://www.eia.gov/outlooks/ieo/pdf/0484\(2016\).pdf](https://www.eia.gov/outlooks/ieo/pdf/0484(2016).pdf); [accessed 20 May 2018].
- 15 [2] U.S. Administration Energy Information. International Energy Outlook 2017,  
16 [https://www.eia.gov/outlooks/ieo/pdf/0484\(2017\).pdf](https://www.eia.gov/outlooks/ieo/pdf/0484(2017).pdf); [accessed 20 May 2018].
- 17 [3] Kriván E, Valkai I, Hancsók J. Investigation of production of motor fuel components on  
18 heterogeneous catalyst with oligomerization. *Top Catal* 2013;56:831–8.
- 19 [4] Bellussi G, Mizia F, Calemma V, Pollesel P, Millini R. Oligomerization of olefins from Light  
20 Cracking Naphtha over zeolite-based catalyst for the production of high quality diesel fuel.  
21 *Microporous Mesoporous Mater* 2012;164:127–34.
- 22 [5] Maseloane MA. Dimerization of naphtha-range Fischer-Tropsch olefins into diesel-range  
23 products over zeolite H-ZSM-5 and amorphous silica-alumina. University of Cape Town,  
24 South Africa, 2011.
- 25 [6] De Klerk A. Distillate production by oligomerization of Fischer-Tropsch olefins over solid

- 1 phosphoric acid. *Energy & Fuels* 2006;20:439–45.
- 2 [7] Bond JQ, Alonso DM, Wang D, West RM, Dumesic JA. Integrated catalytic conversion of  $\gamma$ -  
3 valerolactone to liquid alkenes for transportation fuels. *Science* 2010;327:1110–4.
- 4 [8] Bond JQ, Upadhye AA, Olcay H, Tompsett GA, Jae J, Xing R, et al. Production of renewable  
5 jet fuel range alkanes and commodity chemicals from integrated catalytic processing of  
6 biomass. *Energy Environ Sci* 2014;7:1500–23.
- 7 [9] Alonso DM, Bond JQ, Serrano-Ruiz JC, Dumesic JA. Production of liquid hydrocarbon  
8 transportation fuels by oligomerization of biomass-derived C<sub>9</sub> alkenes. *Green Chem*  
9 2010;12:992–9.
- 10 [10] Nicholas CP. Applications of light olefin oligomerization to the production of fuels and  
11 chemicals. *Appl Catal A Gen* 2017;543:82–97.
- 12 [11] Corma A, Iborra S. Oligomerization of Alkenes. In: Derouane EG, editor. *Catalysts for Fine*  
13 *Chemical Synthesis, Vol. 4, Microporous Mesoporous Solid Catalysts*, John Wiley & Sons;  
14 2006, p. 125–40.
- 15 [12] Sanati M, Hörnell C, Järäs SG. The Oligomerization of Alkenes by Heterogeneous Catalysts.  
16 In: Spivey JJ, editor. *Catalysis: Volume 14*, Cambridge: The Royal Society of Chemistry;  
17 1999, p. 236–87.
- 18 [13] Muraza O. Maximizing diesel production through oligomerization: a landmark opportunity for  
19 zeolite research. *Ind Eng Chem Res* 2015;54:781–9.
- 20 [14] Weitkamp J, Ernst S, Puppe L. Shape-Selective Catalysis. In: Weitkamp J, Puppe L, editors.  
21 *Zeolites. Catalysis and Zeolites. Fundamentals and Applications*, New York: Springer-Verlag  
22 Berlin Heidelberg; 1999, p. 327–76.
- 23 [15] Christensen CH, Johannsen K, Törnqvist E, Schmidt I, Topsøe H, Christensen CH.  
24 Mesoporous zeolite single crystal catalysts: Diffusion and catalysis in hierarchical zeolites.  
25 *Catal Today* 2007;128:117–22.

- 1 [16] Holm MS, Taarning E, Egeblad K, Christensen CH. Catalysis with hierarchical zeolites. *Catal Today* 2011;168:3–16.
- 2
- 3 [17] Weitkamp J. Zeolites and catalysis. *Solid State Ionics* 2000;131:175–88.
- 4 [18] Blauwhoff PMM, Gosselink JW, Kieffer EP, Sie ST, Stork WHJ. Zeolites as Catalysts in Industrial Processes. In: Weitkamp J, Puppe L, editors. *Catalysis and Zeolites*, Berlin: Springer Berlin Heidelberg; 1999, p. 437–538.
- 5
- 6
- 7 [19] Cejka J, Van Bekkum H. Zeolites and Ordered Mesoporous Materials: Progress and Prospects, Volume 157. 1st ed. Elsevier Science; 2005.
- 8
- 9 [20] Corma A. From microporous to mesoporous molecular sieve materials and their use in catalysis. *Chem Rev* 1997;97:2373–419.
- 10
- 11 [21] Chiche B, Sauvage E, Di Renzo F, Ivanova II, Fajula F. Butene oligomerization over mesoporous MTS-type aluminosilicates. *J Mol Catal A Chem* 1998;134:145–57.
- 12
- 13 [22] Pater JPG, Jacobs PA, Martens JA. Oligomerization of hex-1-ene over acidic aluminosilicate zeolites, MCM-41, and silica-alumina co-gel catalysts: A comparative study. *J Catal* 1999;184:262–7.
- 14
- 15
- 16 [23] Tao Y, Kanoh H, Abrams L, Kaneko K. Mesopore-modified zeolites: Preparation, characterization, and applications. *Chem Rev* 2006;106:896–910.
- 17
- 18 [24] Silva AF, Fernandes A, Antunes MM, Neves P, Rocha SM, Ribeiro MF, et al. TUD-1 type aluminosilicate acid catalysts for 1-butene oligomerisation. *Fuel* 2017;209:371–82.
- 19
- 20 [25] Degnan JTF. Applications of zeolites in petroleum refining. *Top Catal* 2000;13:349–56.
- 21 [26] Choudary N V., Newalkar BL. Use of zeolites in petroleum refining and petrochemical processes: recent advances. *J Porous Mater* 2011;18:685–92.
- 22
- 23 [27] Tabak SA, Krambeck FJ, Avidan AA. Production of synthetic gasoline and diesel fuel from non-petroleum resources. *Am Chem Soc, Div Gas Fuel Chem* 1986;31:293–9.
- 24
- 25 [28] Knottenbelt C. Mossgas “gas-to-liquid” diesel fuels - an environmentally friendly option.

- 1 Catal Today 2002;71:437–45.
- 2 [29] Minnie RO. Catalytic conversion of olefins to diesel and gasoline fuel. WO 2006091986 A1,  
3 2006.
- 4 [30] Klerk A de, Furimsky E. Catalysis in the Upgrading of Fischer–Tropsch Syncrude. In:  
5 Furimsky E, editor. Catalysis in the Refining of Fischer–Tropsch Syncrude, Cambridge: Royal  
6 Society of Chemistry; 2010, p. 40–164.
- 7 [31] Lavrenov AV, Karpova TR, Buluchevskii EA, Bogdanets EN. Heterogeneous oligomerization  
8 of light alkenes: 80 years in oil refining. Catal Ind 2016;8:316–27.
- 9 [32] Wulfers MJ, Lobo RF. Assessment of mass transfer limitations in oligomerization of butene at  
10 high pressure on H-beta. Appl Catal A Gen 2015;505:394–401.
- 11 [33] Serrano DP, Escola JM, Pizarro P. Synthesis strategies in the search for hierarchical zeolites.  
12 Chem Soc Rev 2013;42:4004–35.
- 13 [34] Chal R, Gérardin C, Bulut M, van Donk S. Overview and industrial assessment of synthesis  
14 strategies towards zeolites with mesopores. ChemCatChem 2011;3:67–81.
- 15 [35] Zhu K, Zhou X. Manipulating the architecture of zeolite catalysts for enhanced mass transfer.  
16 Curr Opin Chem Eng 2015;9:42–8.
- 17 [36] Pérez-Ramírez J, Christensen CH, Egeblad K, Christensen CH, Groen JC. Hierarchical  
18 zeolites: enhanced utilisation of microporous crystals in catalysis by advances in materials  
19 design. Chem Soc Rev 2008;37:2530–42.
- 20 [37] Corma A, Martínez C, Doskocil E. Designing MFI-based catalysts with improved catalyst life  
21 for C<sub>3</sub>= and C<sub>5</sub>= oligomerization to high-quality liquid fuels. J Catal 2013;300:183–96.
- 22 [38] Wang X, Hu X, Song C, Lux KW, Namazian M, Imam T. Oligomerization of biomass-derived  
23 light olefins to liquid fuel: effect of alkali treatment on the HZSM-5 catalyst. Ind Eng Chem  
24 Res 2017;56:12046–55.
- 25 [39] Amin NAS, Anggoro DD. Dealuminated ZSM-5 zeolite catalyst for ethylene oligomerization

- 1 to liquid fuels. *J Nat Gas Chem* 2002;11:79–86.
- 2 [40] Bertrand-Drira C, Cheng X-wei, Cacciaguerra T, Trens P, Melinte G, Ersen O, et al.  
3 Mesoporous mordenites obtained by desilication: Mechanistic considerations and evaluation  
4 in catalytic oligomerization of pentene. *Microporous Mesoporous Mater* 2015;213:142–9.
- 5 [41] Van Niekerk MJ, O'Connor CT, Fletcher JCQ. Methanol conversion and propene  
6 oligomerization productivity of dealuminated large-pore mordenites. *Ind Eng Chem Res*  
7 1996;35:697–702.
- 8 [42] Yoon JW, Jhung SH, Choo DH, Lee SJ, Lee K-Y, Chang J-S. Oligomerization of isobutene  
9 over dealuminated Y zeolite catalysts. *Appl Catal A Gen* 2008;337:73–7.
- 10 [43] Martínez C, Doskocil EJ, Corma A. Improved THETA-1 for light olefins oligomerization to  
11 diesel: influence of textural and acidic properties. *Top Catal* 2014;57:668–82.
- 12 [44] Wang L, Zhang Z, Yin C, Shan Z, Xiao F-S. Hierarchical mesoporous zeolites with  
13 controllable mesoporosity templated from cationic polymers. *Microporous Mesoporous Mater*  
14 2010;131:58–67.
- 15 [45] Yang Q, Zhang H, Kong M, Bao X, Fei J, Zheng X. Hierarchical mesoporous ZSM-5 for the  
16 dehydration of methanol to dimethyl ether. *Chinese J Catal* 2013;34:1576–1582.
- 17 [46] Serrano DP, Escola JM, Sanz R, Garcia RA, Peral A, Moreno I, et al. Hierarchical ZSM-5  
18 zeolite with uniform mesopores and improved catalytic properties. *New J Chem*  
19 2016;40:4206–16.
- 20 [47] Serrano DP, Aguado J, Morales G, Rodríguez JM, Peral A, Thommes M, et al. Molecular and  
21 meso- and macroscopic properties of hierarchical nanocrystalline ZSM-5 zeolite prepared by  
22 seed silanization. *Chem Mater* 2009;21:641–54.
- 23 [48] Serrano DP, Aguado J, Escola JM, Rodríguez JM, Peral A. Hierarchical zeolites with  
24 enhanced textural and catalytic properties synthesized from organofunctionalized seeds. *Chem*  
25 *Mater* 2006;18:2462–4.

- 1 [49] Wan Z, Wu W, Chen W, Yang H, Zhang D. Direct synthesis of hierarchical ZSM-5 zeolite  
2 and its performance in catalyzing methanol to gasoline conversion. *Ind Eng Chem Res*  
3 2014;53:19471–8.
- 4 [50] Campelo JM, Lafont F, Marinas JM. Pt/SAPO-5 and Pt/SAPO-11 as catalysts for the  
5 hydroisomerization and hydrocracking of n-octane. *J Chem Soc, Faraday Trans*  
6 1995;91:1551–5.
- 7 [51] Li X, Han D, Wang H, Liu G, Wang B, Li Z, et al. Propene oligomerization to high-quality  
8 liquid fuels over Ni/HZSM-5. *Fuel* 2015;144:9–14.
- 9 [52] Al-Dughaiter AS, de Lasa H. HZSM-5 zeolites with different SiO<sub>2</sub>/Al<sub>2</sub>O<sub>3</sub> ratios.  
10 Characterization and NH<sub>3</sub> desorption kinetics. *Ind Eng Chem Res* 2014;53:15303–16.
- 11 [53] Treacy MMJ, Higgins JB. Collection of simulated XRD powder patterns for zeolites. 5th ed.  
12 Elsevier; 2007.
- 13 [54] Góra-Marek K, Derewiński M, Sarv P, Datka J. IR and NMR studies of mesoporous alumina  
14 and related aluminosilicates. *Catal Today* 2005;101:131–8.
- 15 [55] Gallo JMR, Bisio C, Gatti G, Marchese L, Pastore HO. Physicochemical characterization and  
16 surface acid properties of mesoporous [Al]-SBA-15 obtained by direct synthesis. *Langmuir*  
17 2010;26:5791–800.
- 18 [56] Woolery GL, Kuehl GH, Timken HC, Chester AW, Vartuli JC. On the nature of framework  
19 Lewis acid sites in ZSM-5 Brønsted and. *Zeolites* 1997;2449:288–96.
- 20 [57] Silva AF, Fernandes A, Neves P, Antunes MM, Rocha SM, Ribeiro MF, et al. Mesostructured  
21 catalysts based on the BEA topology for olefin oligomerisation. *ChemCatChem*  
22 2018;10:2741-2754. doi:10.1002/cctc.201701597.
- 23 [58] Harandi MN, Owen H. Integrated staged conversion of methanol to gasoline and distillate. US  
24 4899002 A, 1988.
- 25 [59] Tabak SA, Krambeck FJ, Garwood WE. Conversion of propylene and butylene over ZSM-5

- 1 catalyst. *AIChE J* 1986;32:1526–31. doi:10.1002/aic.690320913.
- 2 [60] Yates JG, Rowe PN, Whang ST. The isomerization of n-butenes over a fluidised silica-  
3 alumina catalyst. *Chem Eng Sci* 1970;25:1387–94.
- 4 [61] Sarazen ML, Duskocil E, Iglesia E. Effects of void environment and acid strength on alkene  
5 oligomerization selectivity. *ACS Catal* 2016;6:7059–70.
- 6 [62] Kumar N, Mäki-Arvela P, Yläsalmi T, Villegas J, Heikkilä T, Leino AR, et al. Dimerization  
7 of 1-butene in liquid phase reaction: Influence of structure, pore size and acidity of Beta  
8 zeolite and MCM-41 mesoporous material. *Microporous Mesoporous Mater* 2012;147:127–  
9 34.
- 10 [63] Keim W, Hoffmann B, Lodewick R, Peuckert M, Schmitt G, Fleischhauer J, et al. Linear  
11 oligomerization of olefins via nickel chelate complexes and mechanistic considerations based  
12 on semi-empirical calculations. *J Mol Catal* 1979;6:79–97.
- 13 [64] Henry M, Bulut M, Vermandel W, Sels B, Jacobs P, Minoux D, et al. Low temperature  
14 conversion of linear C4 olefins with acid ZSM-5 zeolites of homogeneous composition. *Appl*  
15 *Catal A, Gen* 2012;413–414:62–77.
- 16 [65] O'Connor CT, Forrester RD, Scurrill MS. Cetane number determination of synthetic diesel  
17 fuels. *Fuel* 1992;71:1323–7.
- 18 [66] Kapur GS, Ecker A, Meusinger R. Establishing quantitative structure-property relationships  
19 (QSPR) of diesel samples by proton-NMR & multiple linear regression (MLR) analysis.  
20 *Energy and Fuels* 2001;15:943–8.
- 21
- 22 [67] de Klerk A. Can Fischer-Tropsch syncrude be refined to on-specification diesel fuel? *Energy*  
23 *& Fuels* 2009;23:4593–604.
- 24 [68] de Lasa H, Dogammau G, Ravella A. Fuels of the future and changing fuel needs. In: de Lasa  
25 H, Dogammau G, Ravella A, editors. *Reactor Technology for Environmentally Safe Reactors*

- 1 and Products, Springer Netherlands; 1992, p. 1–182.
- 2 [69] Leckel D. Diesel production from Fischer-Tropsch: the past, the present, and new concepts.  
3 Energy & Fuels 2009;23:2342–58.
- 4 [70] De Klerk A. Fischer–Tropsch refining: technology selection to match molecules. Green Chem  
5 2008;10:1249–79.
- 6 [71] Schwarz S, Kojima M, O’Connor CT. Effect of silicon-to-aluminium ratio and synthesis time  
7 on high-pressure olefin oligomerization over ZSM-5. Appl Catal 1989;56:263–80.
- 8 [72] Li C, Du J, Wang H, Li X, Zhu SS, Liu G, et al. A hemicellulose modified HZSM-5 and their  
9 application in the light olefins oligomerization to high-quality liquid fuels reaction. Catal  
10 Commun 2017;102:89–92.
- 11 [73] Yoon JW, Chang J-S, Lee H-D, Kim T-J, Jung SH. Trimerization of isobutene over a zeolite  
12 beta catalyst. J Catal 2007;245:253–6.
- 13 [74] Yoon JW, Lee JS, Jung SH, Lee K-Y, Chang J-S. Oligomerization of isobutene over  
14 aluminum chloride-loaded USY zeolite catalysts. J Porous Mater 2009;16:631–4.
- 15 [75] Mafra L, Vidal-Moya JA, Blasco T. Structural Characterization of Zeolites by Advanced Solid  
16 State NMR Spectroscopic Methods. vol. 77. 2012.
- 17 [76] Wiper P V, Amelse J, Mafra L. Multinuclear solid-state NMR characterization of the  
18 Brønsted/Lewis acid properties in the BP HAMS-1B (H-[B]-ZSM-5) borosilicate molecular  
19 sieve using adsorbed TMPO and TBPO probe molecules. J Catal 2014;316:240–50.
- 20 [77] Hayashi S, Jimura K, Kojima N. Microporous and Mesoporous Materials Acid property of  
21 MFI-type zeolites probed by trimethylphosphine oxide studied by solid-state NMR.  
22 Microporous Mesoporous Mater 2014;186:101–5.
- 23  
24  
25



1 **Figure Captions**

2 **Figure 1.** Flow diagram of the lab-scale catalytic reactor setup. A – 1-Butene cylinder, B – Nitrogen  
 3 cylinder, C - Mass flow controller, D - Syringe pump, E – Relief valve (Parker), F - Fixed-bed  
 4 reactor, G - Tubular oven, H - Back-pressure regulator, I - Jacketed cooling trap, J - Gas  
 5 chromatograph.

6 **Figure 2.** PXRD patterns for hZSM-5(31)-noT (a), hZSM-5(20)-PZSi (b), hZSM-5(51)-PZSi (c),  
 7 hZSM-5(47)-PZSiS (d), hZSM-5(31)-CoT (e), and ZSM-5(29) (f).

8 **Figure 3.** SEM (left column, a,d,g,j,m,p) and STEM (middle and right columns) images of hZSM-  
 9 5(31)-noT (a, b, c), hZSM-5(20)-PZSi (d, e, f), hZSM-5(51)-PZSi (g, h, i), hZSM-5(47)-PZSiS (j, k,  
 10 l), hZSM-5(31)-CoT (m, n, o), and ZSM-5(29) (p, q, r).

11 **Figure 4.** Pore size distribution curves (DFT method) for hZSM-5(31)-noT (a, b), hZSM-5(20)-PZSi  
 12 (c, d), hZSM-5(51)-PZSi (e, f), hZSM-5(47)-PZSiS (g, h), and hZSM-5(31)-CoT (i, j).

13 **Figure 5.** Conversion (\*) and STY (bars) of NCut (dark colour) and DCut (light colour) products for  
 14 the MFI-based materials prepared and the benchmark catalyst ZSM-5(29). Reaction conditions: 200  
 15 °C, 30 bar,  $WHSV=2.2 \text{ g}_{1C4} \text{ g}_{cat}^{-1} \text{ h}^{-1}$ , TOS = 7 h, catalyst activation temperature = 450 °C.

16 **Figure 6.** PLD profiles for the liquid products of the reaction of 1-butene in the presence of the MFI-  
 17 based materials: (a) hZSM-5(20)-PZSi (solid line), hZSM-5(51)-PZSi (dashed line), hZSM-5(47)-  
 18 PZSiS (dotted line), and (b) hZSM-5(31)-noT (solid line), hZSM-5(31)-CoT (dashed line), and  
 19 ZSM-5(29) (dotted line). Reaction conditions: 200 °C, 30 bar,  $WHSV=2.2 \text{ g}_{1C4} \text{ g}_{cat}^{-1} \text{ h}^{-1}$ , TOS = 7 h,  
 20 catalyst activation temperature = 450 °C.

21 **Figure 7.** STY as a function of  $X_{C4}$  for the different catalysts prepared (STY total (●), STY DCut  
 22 (×), and STY NCut (+)). Reaction conditions: 200 °C, 30 bar,  $WHSV=2.2 \text{ g}_{1C4} \text{ g}_{cat}^{-1} \text{ h}^{-1}$ , TOS = 7 h,  
 23 catalyst activation temperature = 450 °C.

1 **Figure 8.** Influence of the acid properties measured at 200 °C on  $X_{C4}$  ( $\times$ ), (a, b),  $STY_{DCut}$  ( $\blacksquare$ ) and  
2  $STY_{NCut}$  ( $\square$ ) (c, d), for the catalysts prepared according to the PZSi(S) protocols, namely hZSM-  
3 5(20)-PZSi, hZSM-5(51)-PZSi, and hZSM-5(47)-PZSiS. Reaction conditions: 200 °C, 30 bar,  
4  $WHSV=2.2 \text{ g}_{IC4} \text{ g}_{cat}^{-1} \text{ h}^{-1}$ , TOS = 7 h, catalyst activation temperature = 450 °C.

5 **Figure 9.** Dependence of conversion ( $X_{C4}$ ) on TOS for hZSM-5(20)-PZSi (A), hZSM-5(51)-PZSi  
6 (C) and ZSM-5(29) (E) in the first ( $\times$ ) and second cycle using the regenerated catalyst (-). PLD  
7 curves for the two cycles (with matching symbols) for hZSM-5(20)-PZSi (B), hZSM-5(51)-PZSi (D)  
8 and ZSM-5(29) (F).

9 **Figure 10.** PXRD patterns (A) and  $^{27}\text{Al}$  MAS NMR spectra (B) for hZSM-5(20)-PZSi (fresh (a);  
10 used (b)), hZSM-5(51)-PZSi (fresh (c); used (d)), and ZSM-5(29) (fresh (e); used (f)).

11

**Table 1.** Protocols and synthesis conditions of the zeotypes based on the MFI topology.

Synthesis step	noT	PZSi	CoT
Synthesis mixture	TEOS, TPAOH <sup>a</sup> , NaAlO <sub>2</sub> , H <sub>2</sub> O (50) <sup>b</sup>	TEOS, TPAOH, AiP, H <sub>2</sub> O (30 and 60) <sup>b</sup>	TEOS, TPAOH, NaAlO <sub>2</sub> , H <sub>2</sub> O (36) <sup>b</sup>
Aging (with stirring)	20 h, aT <sup>c</sup>	44 h/aT <sup>c</sup> ; 22 h/90 °C	3 h, 100 °C
Additional template	None	PHAPTMS, 90 °C/6 h	PDD-AM, aT <sup>c</sup> /15 h
Hydrothermal treatment	180 °C, 2 d <sup>d</sup> , static	170 °C, 7.7 d <sup>d</sup> , static	180 °C, 6 d <sup>d</sup> , static
Centrifugation, wash, dry	100 °C	110 °C	100 °C
Calcination	550 °C/5 h	550 °C/5 h	550 °C/5 h
Ion-exchange; calcination	(3×) 1.0 M NH <sub>4</sub> NO <sub>3</sub> , 50 °C/24 h; 500 °C/5 h	None	(3×) 1.0 M NH <sub>4</sub> NO <sub>3</sub> , 80 °C/2 h; 550 °C/4 h
Sample name	hZSM-5(31)-noT	hZSM-5(x)-PZSi <sup>e</sup>	hZSM-5(31)-CoT

<sup>(a)</sup> TPAOH as the structure-directing agent accounting for the hierarchical features. <sup>(b)</sup> Si/Al ratio of the synthesis gel. <sup>(c)</sup> aT = ambient temperature. <sup>(d)</sup> d = days. <sup>(e)</sup> x is the molar ratio Si/Al of the final material (x = 20 or 51).

**Table 2.** Elemental analyses and textural properties of the MFI-based materials.<sup>a</sup>

Sample	Si/Al <sup>a</sup>	Textural properties						
		$S_{\text{BET}}$ ( $\text{m}^2\text{g}^{-1}$ )	$S_{\text{meso}}^{\text{b}}$ ( $\text{m}^2\text{g}^{-1}$ )	$\%S_{\text{meso}}$	$V_{\text{p}}$ ( $\text{cm}^3\text{g}^{-1}$ )	$V_{\text{micro}}^{\text{c}}$ ( $\text{cm}^3\text{g}^{-1}$ )	$\%V_{\text{micro}}$	$D_{\text{p}}^{\text{d}}$ (nm)
hZSM-5(31)-noT	31	308	168	54	0.46	0.04	8	2-10
hZSM-5(20)-PZSi	20	721	308	43	0.74	0.09	12	2-5
hZSM-5(51)-PZSi	51	558	289	52	0.77	0.07	10	2-7
hZSM-5(47)-PZSiS	47	464	275	59	0.76	0.05	7	2-5
hZSM-5(31)-CoT	31	853	140	16	0.48	0.25	52	2-5
ZSM-5(29)	29	334	97	29	0.47	0.17	36	-

<sup>a</sup> Molar ratio determined by EDS. <sup>b</sup> External/mesoporous specific surface area. <sup>c</sup>

Micropore volume (calculated for  $p/p_0 \approx 0.99$ ). <sup>d</sup> Mesopore size range. For all materials, the micropore size distribution (based on DFT) indicated a median pore size in the range 0.55-0.57 nm.

**Table 3.** Al-species and acid properties of the MFI-based materials.

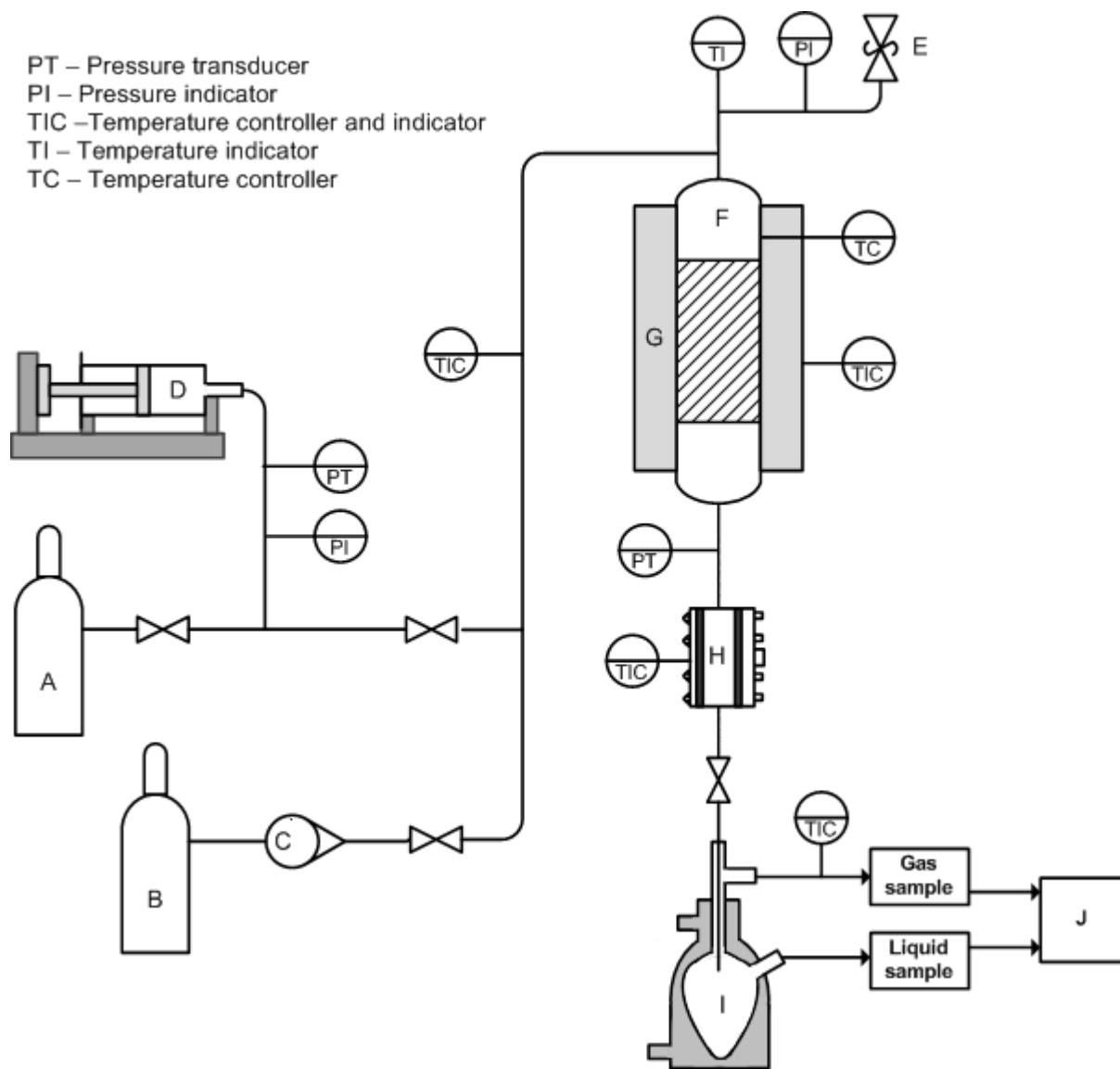
Sample	Al species <sup>a</sup>		Acid properties <sup>b</sup>			
	% Al <sub>tetra</sub>	% Al <sub>oct</sub>	L+B ( $\mu\text{mol g}^{-1}$ )	L/B	L <sub>450</sub> /L <sub>200</sub>	B <sub>450</sub> /B <sub>200</sub>
hZSM-5(31)-noT	91	9	252	0.19	1.01	0.25
hZSM-5(20)-PZSi	75	25	251	1.34	0.47	0.06
hZSM-5(51)-PZSi	81	19	132	0.59	0.61	0.04
hZSM-5(47)-PZSiS	93	7	147	0.33	0.59	0.04
hZSM-5(31)-CoT	88	12	152	0.26	1.02	0.14
ZSM-5(29)	94	6	365	0.22	0.85	0.21

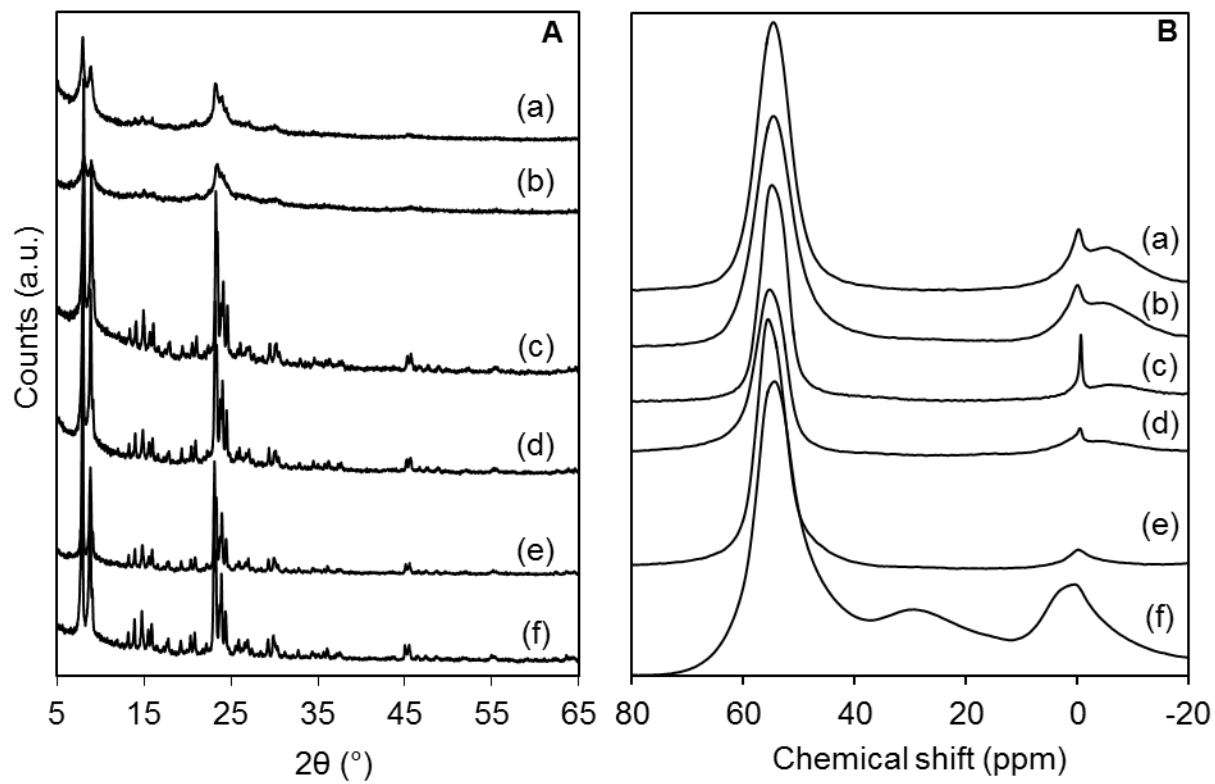
<sup>a</sup> Determined by <sup>27</sup>Al MAS NMR spectroscopy. <sup>b</sup> Determined by FT-IR of pyridine

adsorbed at 200 °C; B=Brönsted acid sites, L=Lewis acid sites, B+L=total amount of acid sites.

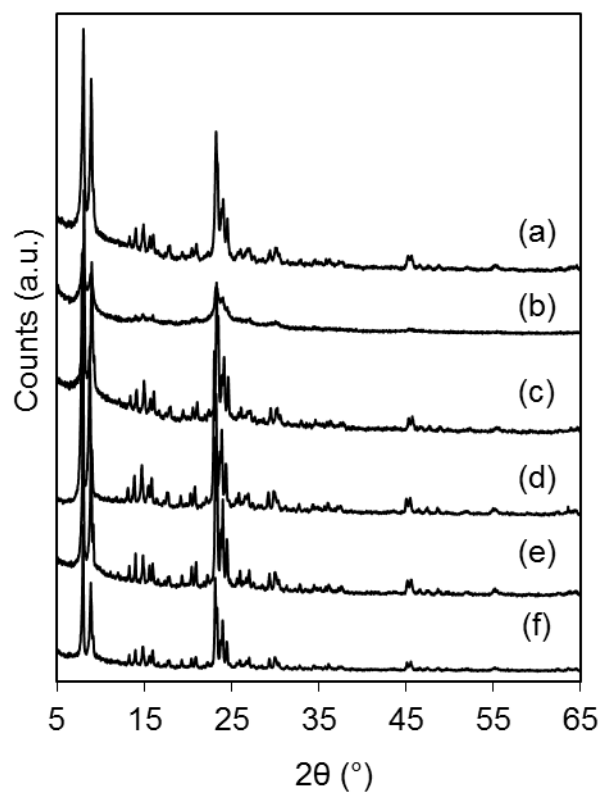
**Table 4.** Influence of the catalyst activation temperature ( $T_{act}$ ) and reaction conditions (T, P) on the catalytic reaction.

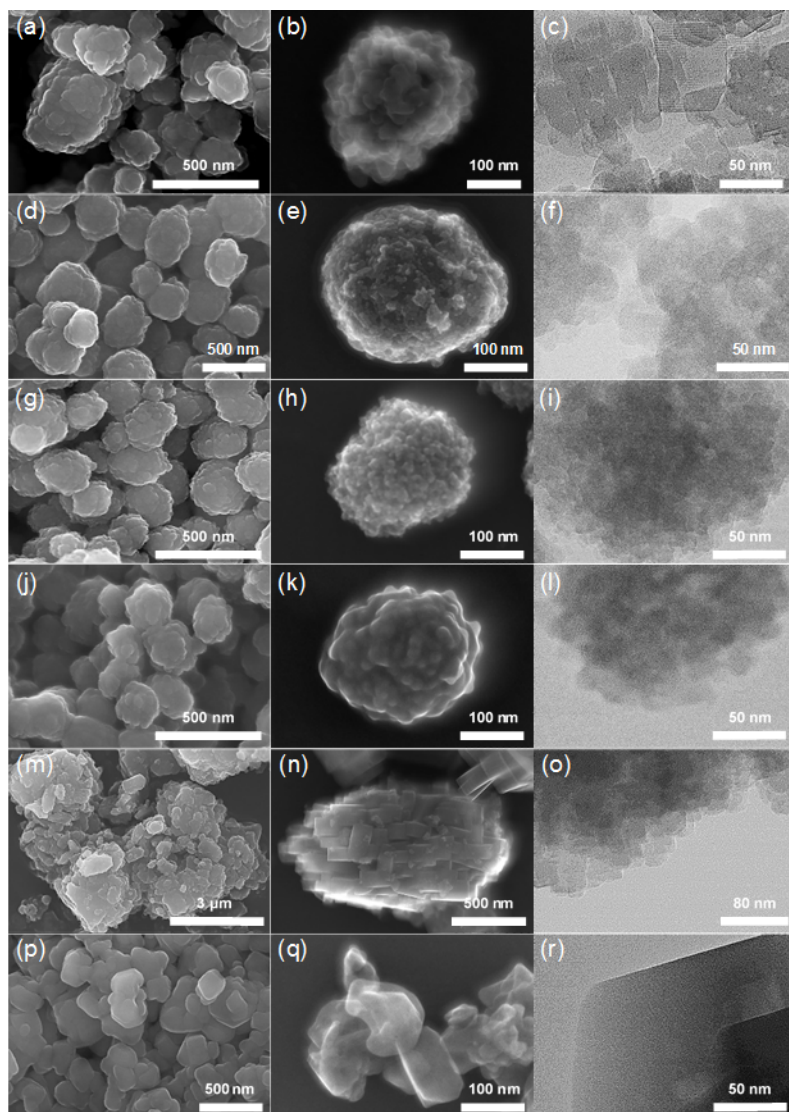
Conditions			$X_{C4}$ (%)	STY (mg. g <sup>-1</sup> h <sup>-1</sup> )			DCut/NCut
$T_{act}$ (°C)	T (°C)	P (bar)		NCut	DCut	Total	
200	200	30	77	272	543	815	2.0
450	200	30	77	257	534	791	2.1
450	250	30	87	414	611	1025	1.5
450	250	40	97	408	669	1077	1.6

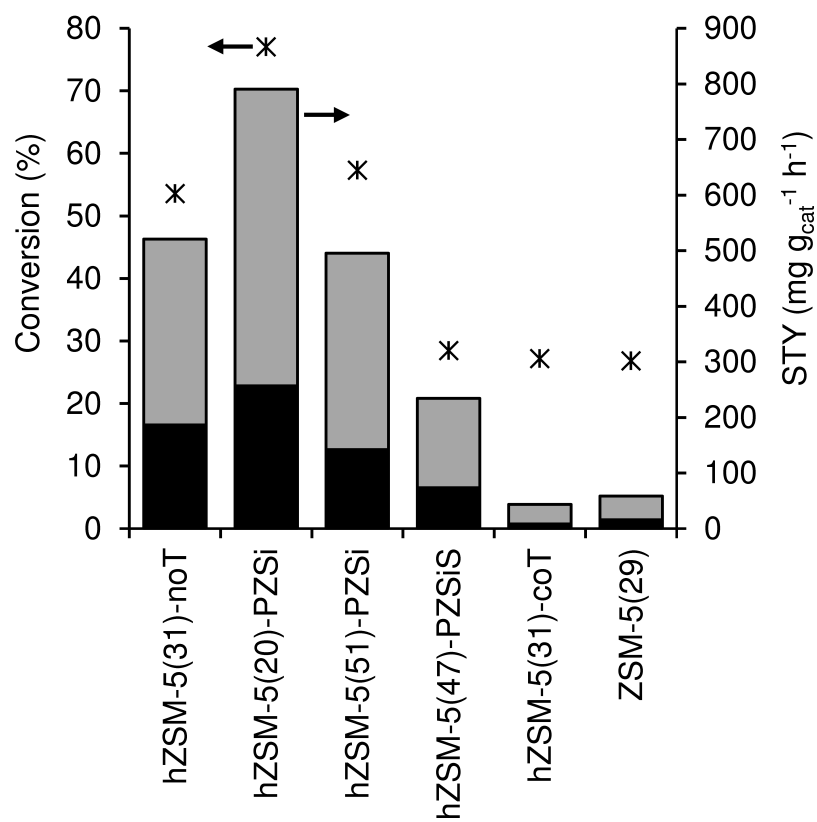


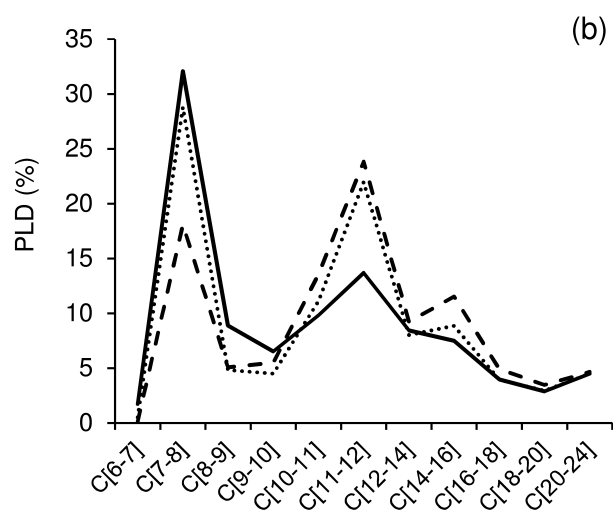
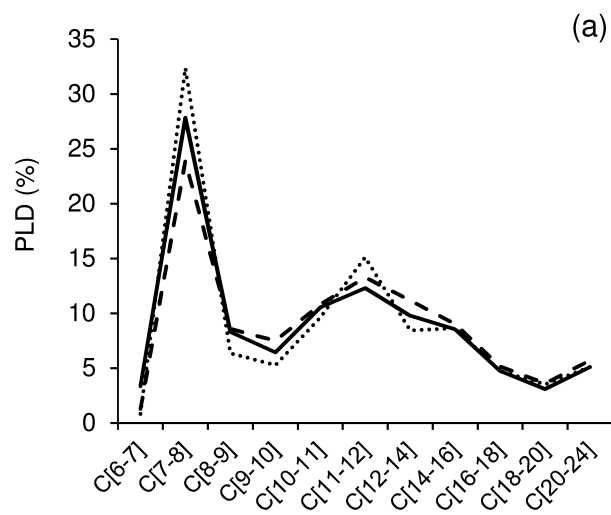


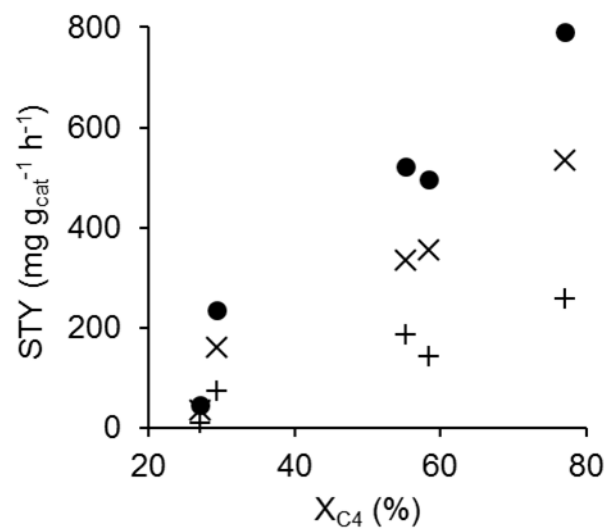


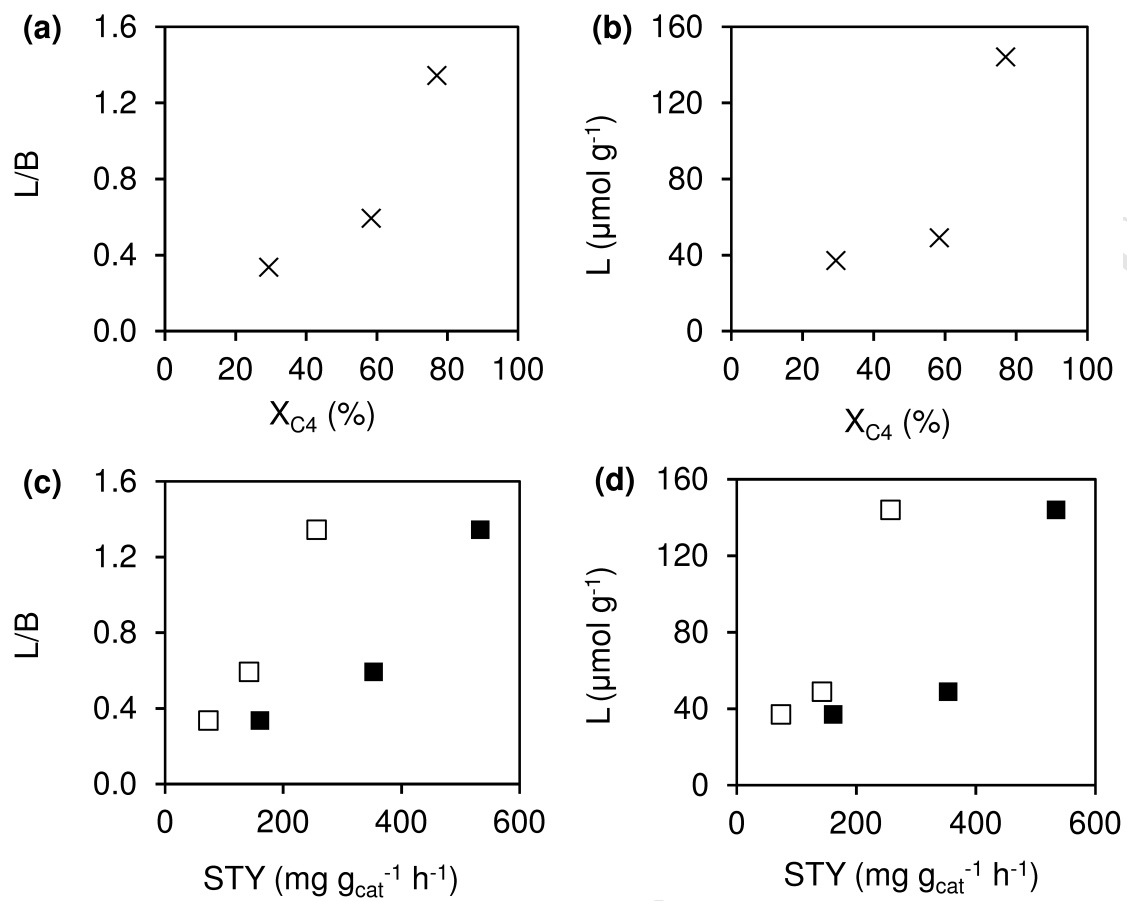


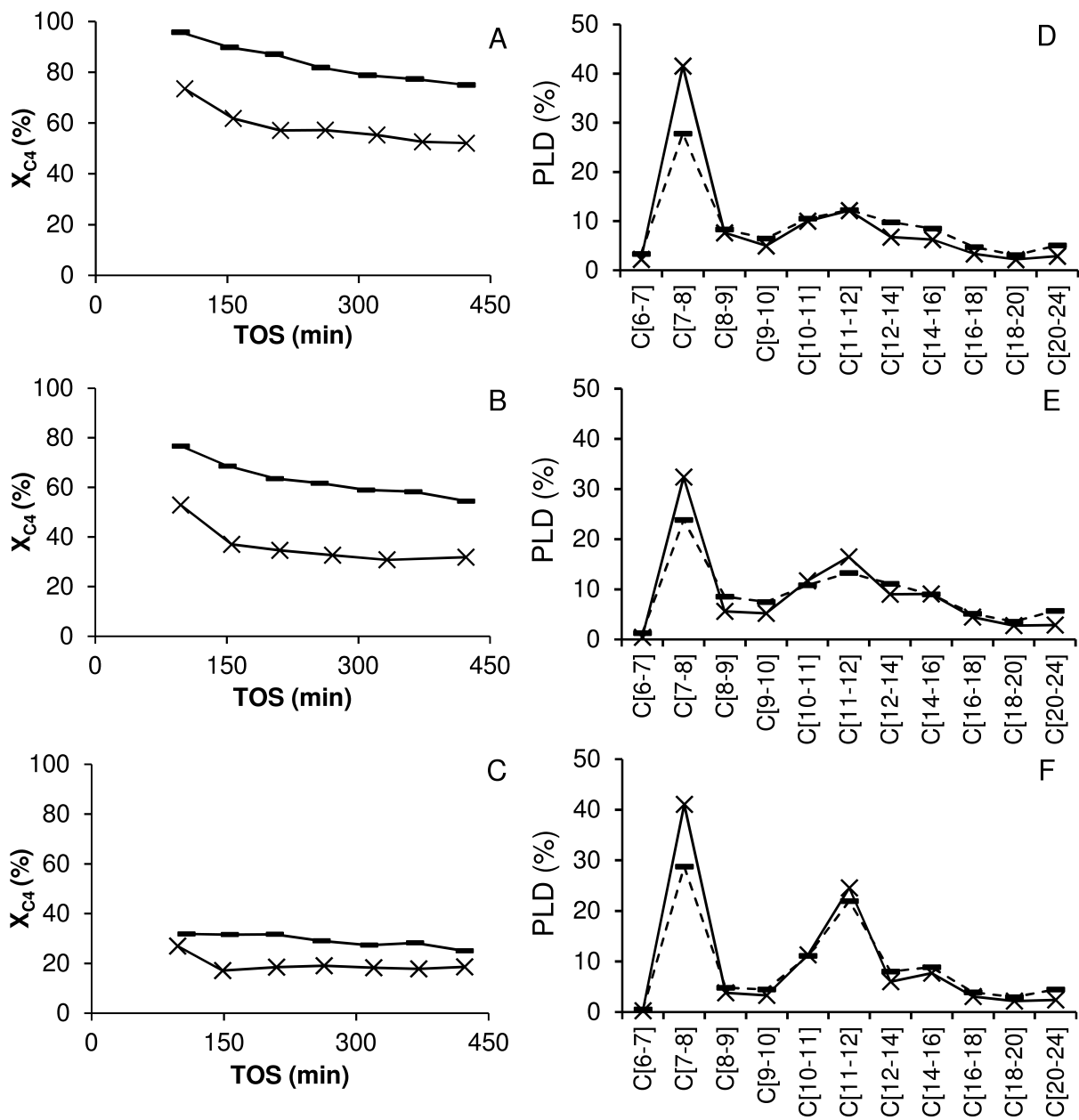




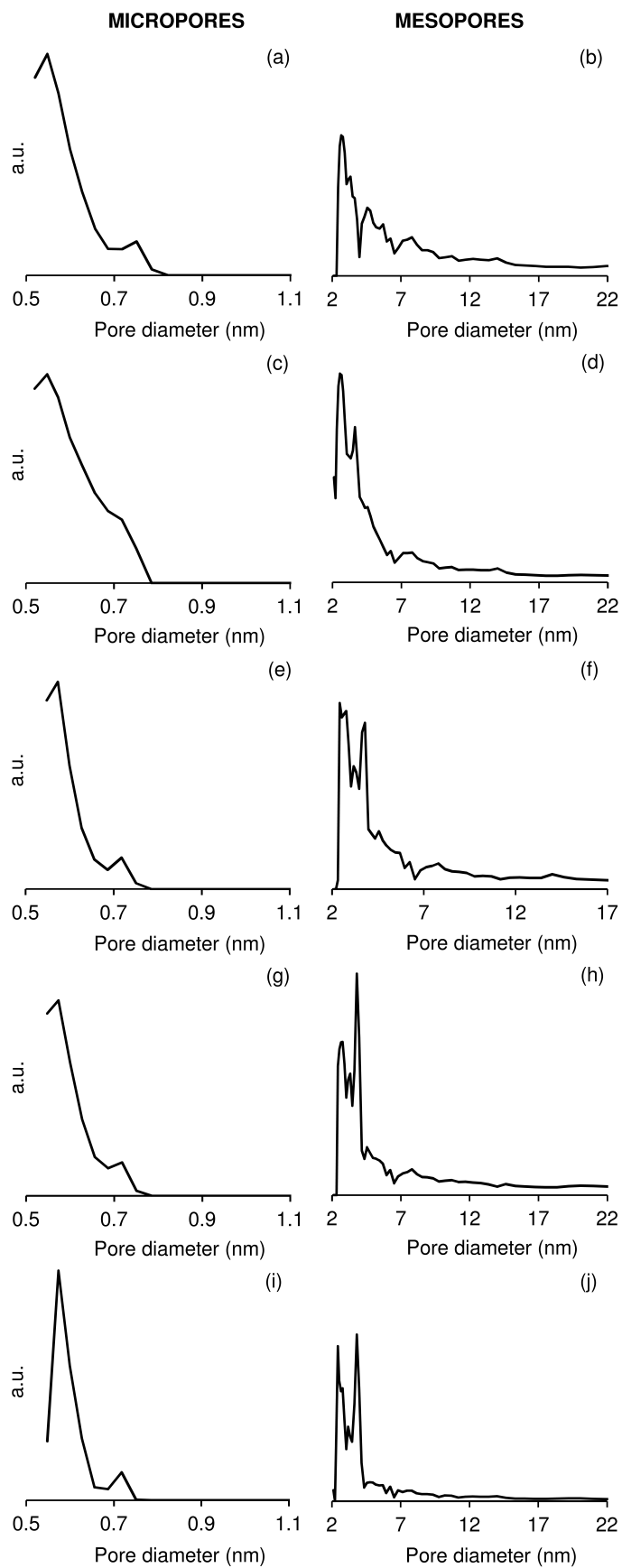








ACC





**Highlights**

Olefins to diesel type products via oligomerisation over MFI-based catalysts

Non-destructive synthetic bottom-up approaches to micro/mesoporous nano-zeotypes

Regular morphology, nanocrystallites, mesoporosity, L/B favour catalytic performance

Zeotypes outperformed commercial ZSM-5 which possessed greater amount of acid sites

ACCEPTED MANUSCRIPT